Chapter 2
The Phenomena of Non-Proportionality in Loading Fatigue

Abstract Chapter presents the influence of non-proportionality on various physical phenomena that accompany the fatigue process, and they include the formation of specific properties in the microstructure of metals, the resulting strengthening of material, the initiation and development of cracks, and last but not least, the influence of non-proportionality on important exploitation features of machine parts as well as fatigue life and strength.

Keywords Dislocations structures · Development of cracks · Fatigue life and strength · Additional cyclic hardening

The fatigue process includes many phases based on different mechanisms of material damage. There are at least 4 stages of the fatigue accumulation process in fatigue damage as follows: (1) initiation during which persistent slip bands and cracks nucleate at the surface or within grain boundaries are formed, (2) the I stage understood as initial short crack propagation on the maximum shear stress plane across a couple of grains, (3) the development of fracture in the II stage long crack propagation takes place of normal to the global principal tensile stress, and (4) final fracture. The non-proportional loading influences the course of each of these stages, causing qualitative and even quantitative changes in the properties of the fatigue process.

In this chapter, an attempt is made to describe in what way the non-proportionality of loading influences the microstructure of the material (slip bands and dislocations structures) and how it results in a change of the relationship between stress and strain during plastic strain (slip bands and dislocations structures). The results of thermographic analyses are shown which were conducted in non-proportional stress conditions. The influence of non-proportional loading on the development of short cracks (their distribution) and long cracks (propagation rate and path) is described. The chapter ends with a description of how eventually non-proportionality influences the exploitation parameters such as fatigue life and strength. Moreover, the appearance of fatigue fracture faces that resulted from non-proportional loading will be discussed.

D. Skibicki, *Phenomena and Computational Models of Non-Proportional Fatigue of Materials*, SpringerBriefs in Computational Mechanics,
DOI: 10.1007/978-3-319-01565-1_2, © The Author(s) 2014

2.1 The Influence of Non-Proportionality on the Microstructure of Metals

2.1.1 Slip Bands

The differences in the microstructure caused by loading of different levels of non-proportionality have been by Mcdowell et al. (1988). A specimen marked SS09 (Fig. 2.1a) was exposed to a high degree non-proportional loading. Due to this, a maximum number of slip systems for biaxial loading were activated in the sample material. However, on the SS06 specimen, which was exposed only to alternating pure axial and pure torsion blocks, usually only one slip system per grain is noticeable (Fig. 2.1b).

Liu and Wang (2001) present slip bands for steel 316 with tension and torsion loading, in phase and with phase shift of 90°. For the in-phase loading, the directions of slip bands coincide with the maximum values of the failure parameter suggested by the authors (Fig. 2.2a). These directions are located at 20° counter clockwise and 70° clockwise from the longitudinal axis (white arrow). In the case of non-proportional loading, the direction of the plane on which the maximum value of the failure parameter is 75° clockwise (Fig. 2.2b). The directions of the slip bands for non-proportional loading are less consistent with the critical plane. The authors explain this by saying that it is related to the characteristic of the damage parameter distribution—in the area of its maximum value (within ±5°) the distribution of values is approximately uniform.

Zhang and Jiang (2005) conducted studies comparing slip bands and dislocation substructures of copper produced in proportional loading, torsion, and tension-compression with those produced in non-proportional loading caused by torsion, and tension-compression with the component phase shift equal to 90°. Even for large loading values, there were at most only two slip systems activated in proportional loading (Fig. 2.3a). Their specific property is the dominance of one of those systems. In non-proportional loading, other slip systems are also activated. These systems were equal and common in each grain (Fig. 2.3b).

These examples above show that, under the influence of non-proportional loading, as a result of shear stress acting in multiple planes and in multiple directions, there are many more slip systems activated than in uniaxial or multiaxial proportional loading.

2.1.2 Dislocations Structures

Dislocation structures formed as a result of proportional loading fatigue have been described and classified extensively (Kocanda 1978). The type of a given structure depends on many factors related to material and loading. The material parameters include a type of crystalline structure and the value of the stacking fault energy

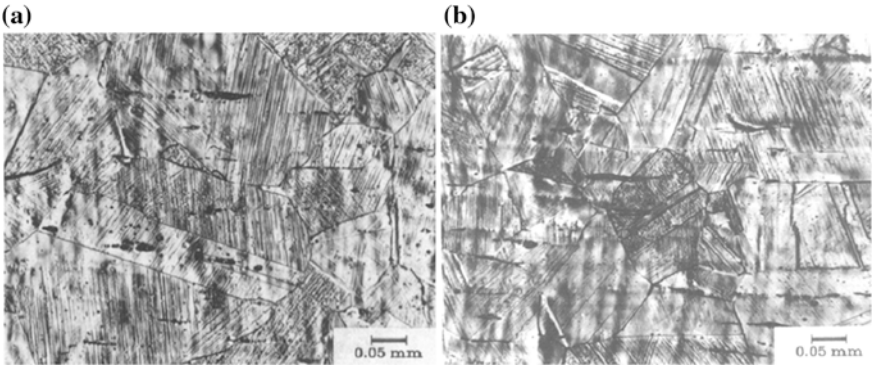

Fig. 2.1 Slip band for specimens. **a** SS09 **b** SS06 (Mcdowell et al. 1988)

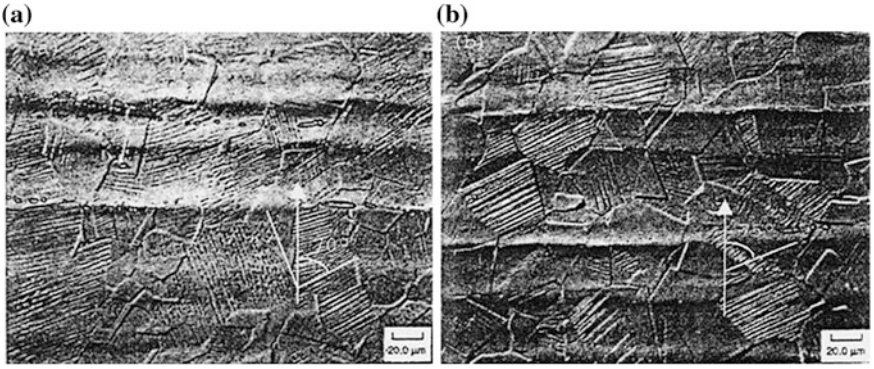

Fig. 2.2 Slip band for: **a** in-phase path, **b** 90° out-of-phase path (Liu and Wang 2001)

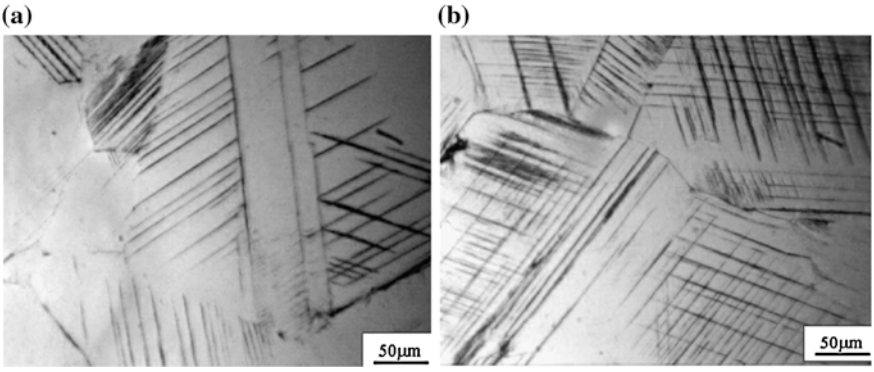

Fig. 2.3 Slip bands on the surface: **a** tension-compression, **b** tension-compression with torsion, with phase shift 90° (Zhang and Jiang 2005)

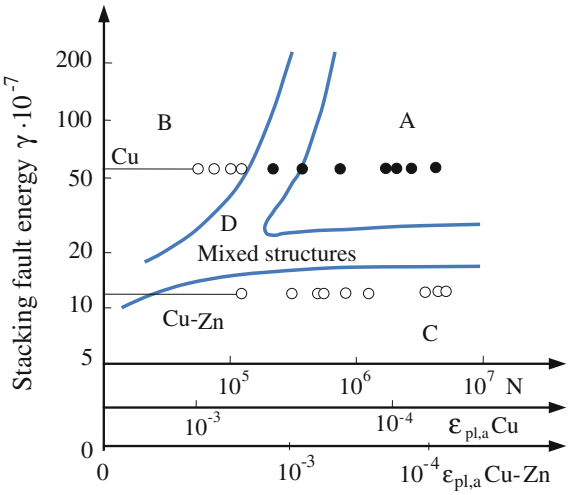

Fig. 2.4 A diagram of the relationship between the type of dislocation structure in metals with face-centred cubic cell and SFE and the number of loading cycles N and the value of plastic strain (Kocanda 1978)

(SFE). As far as loading is concerned, its values are important and, in the case of cyclic loading, the number of loading cycles is important.

Figure 2.4 shows the relationship between the types of dislocation structures and the SFE values, the number of fatigue cycles, and the value of the amplitude of plastic strain (Kocanda 1978). The figure shows that, for the high cycle loading and for high value SFE metals, dislocation bundles and veins are typical. In Fig. 2.4, this area was marked as "A." In area "B," which represents low cycle loading and high SFE value metals, cell structures occur. Area "C," indicates that there are bands of flat dislocation systems (also called band dislocation structures), which are typical for metals with low SFE values. Mixed structures occur in area "D." In Fig. 2.4, the evolution of dislocation structures of CU in a CU–Zn alloy is depicted against the background of the areas described above. These structures change together with an increase in the number of fatigue cycles. A distinctive feature of these changes is that in the Cu–Zn alloy, due to a lower SFE value, no cell structures occur, while in Cu they develop over time.

Kocanda (1978) summarises the distinctive cell features of dislocation structures occurring in cyclic loading fatigue. With an increase of the loading amplitude, cell sizes decrease. Moreover, with an increase in cycles, the following changes take place:

- The sharpness (definition) of the cell walls increases.
- Cell disorientation increases.
- Dislocation is removed from the inside of the cells.
- Dislocation structures develop inwards.

The research on dislocation structures in reference to non-proportional loading is extensive. However, there is a need for a systematic approach to this problem as has been done for uniaxial proportional loading.

Nishino et al. (1986) conducted two very interesting experiments in sequential loading, and he studied the response of the material in dislocation structures.

The first experiment consisted in observing dislocation structures at the temperature of 823 K and with 1 % strain for three types of loading: (a) tension-compression, (b) torsion, and (c) loading with consecutive cycles of tension-compression and torsion. For uniaxial loading, which is for tension-compression and torsion, the dislocation structures were very similar, and they were ladder or maze structures. One needs to note that, at room temperature, with these levels of strain, cellular structures would develop (Nishino et al. 1986). However, at a high temperature, dislocation structures could transform into structures of lower energy (Nishino et al. 1986). However, the situation was different in non-proportional loading. In this case, the plane of maximum stress changed by 45° between stress blocks. In these conditions, in spite of the high temperature, cellular structure developed. According to Nishino, an increase in the dislocation interaction that come from many activated slip systems made it impossible for the cellular structure to transform a ladder or maze structure. Naturally, it resulted in additional hardening. In relations to uniaxial loading—tension-compression and torsion—it reached the high value of 40 %.

Nishino's second experiment (Nishino et al. 1986) consisted in causing fatigue failure of the sample by applying a two-block loading programme: initial tension and subsequent torsion. The change in the type of loading was in-phase, when the hardening curve reached its saturation state. At the point of change in loading, there occurred further rapid, additional hardening, which is termed *cross hardening*. In time, the value of hardening returned to its previous stable value. The dislocation structures under study after the completion of the experiment turned out to be equivalent to the dislocation structures typical for pure torsion. The dislocations were distributed in planes of maximum shear stress. This means that, in the initial phase of the torsion block, some reorganizing of the dislocation structures took place. This was accompanied by hardening. At the point of change in the type of loading, when he previous dislocation structure still existed while the new one was just beginning to form, the strong interaction between the locations was evident with differently oriented slip systems.

Mcdowell et al. (1988) analysed differences in deformation substructures for samples for which the slip systems are presented in Fig. 2.1. Figure 2.5a shows specimen SS09 with a loading of a higher degree of non-proportionality, while Fig. 2.5b shows specimen SS01 with a lower degree of non-proportionality. A comparison of these two photographs reveals that dislocation cells in SS09 are smaller; moreover, the dislocations fill the inside of the cells, while in SS01, the inside of the cells is empty (without dislocation).

Rios et al. (1989) in their research on the influence of non-proportional loading on steel 316 noted that this loading causes a change in the nature of the dislocation cell walls from loosely tangled in proportional loading into a tight, thick maze in

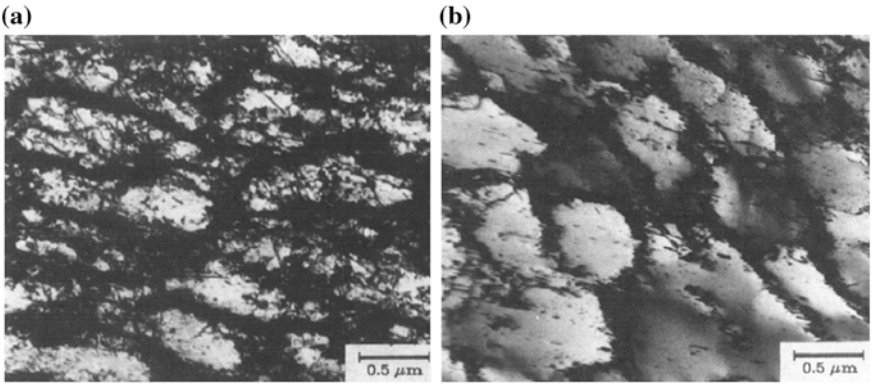

Fig. 2.5 Slip systems for specimens: **a** SS09, **b** SS01 (Mcdowell et al. 1988)

non-proportional loading. The walls of the cells become sharper and have a greater disorientation angle. The dislocation concentration increases when measured on the cell walls as well as on the entire area under investigation. Rios was searching for a relationship between the influence of the degree of non-proportionality and the value of the monotonic loading amplitude and its influence on the development of dislocation structures. According to him, the image of dislocation structures for large monotonic plastic strain is similar to the structures formed in non-proportional loading.

Jiao et al. (1995) studied how the number of active slip systems in proportional loading increases in non-proportional loading in 800H alloy. The concentration of dislocation increased and their distribution was more uniform.

Xiao and Kuang (1996) researched dislocation structures for steel 302 in non-proportional loading with different degrees of non-proportionality. They noted that, for the same degree of loading, with an increase in non-proportionality, the dislocation structures changed from a vein structure for the "double triangle" loading path, through the elongated cell structure—elliptical loading, to well-developed dislocation cells for the circular loading path. With an increase of non-proportionality of loading, the structures took on the forms equivalent to proportional loading structures with continually decreasing strengths (that is for continually increasing loading amplitudes). It means that the damaging character of non-proportional loading can be correlated with the increase of the degree of non-proportionality as defined by the analysis of the loading path.

Kida et al. (1997) described changes in dislocation structures of steel 304 that occurred as a result of 13 different loading cases, including 11 non-proportional. They noticed that, as a result of principal axes rotation, many dislocations can be found inside the dislocation cells. The authors analysed the occurrence of certain types of dislocation structures as a function of the principal strain range value and the non-proportional factor. They stated that there exists a critical boundary separating dislocation bundles and forming cells. In Fig. 2.6, this boundary is marked

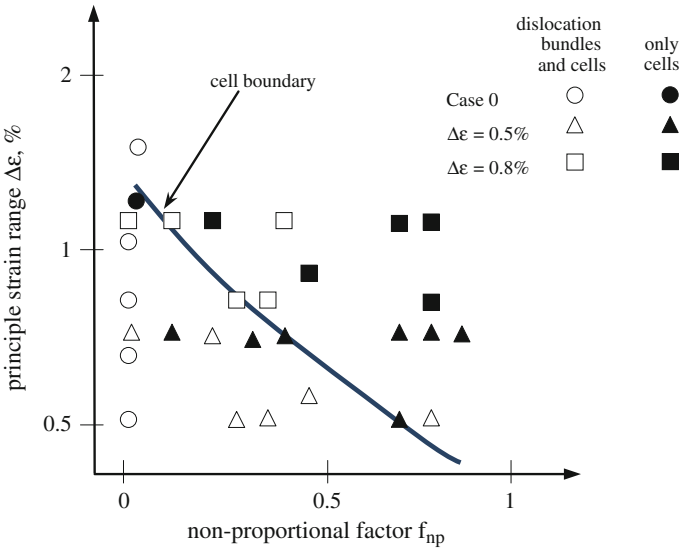

Fig. 2.6 The influence of the principal strain range and the non-proportional factor on dislocation structures (Kida et al. 1997)

with a solid line. The analysis of dislocation structures formed in uniaxial loading, that is Case 0 (on the X-axis the value of non-proportional factor $f_{np} = 0$), shows that cell formation was observed in the specimens loaded at large strain ranges (at least 1 %), and dislocation bundles were observed at lower strain ranges. These results have been marked in Fig. 2.9 with small circles. With the increase of the degree of non-proportionality, the value of the principal strain range required for the formation of cell structures decreases.

Xiao et al. (2000) conducted studies for A3 lattice material—Zircaloy-4. The results are similar to those described earlier (Xiao and Kuang 1996). In non-proportional loading of a lower value ($\varepsilon = 0.8$ %), cellular structures formed that were identical to those in proportional loading with a higher value ($\varepsilon = 1.146$ %).

Bocher et al. (2001) analysed dislocation structures of austenitic steel 316 exposed to proportional and non-proportional loading. Under the influence of proportional loading, dislocation structures appear in the form of tangles or uncondensed cells (Fig. 2.7a). Under the influence of non-proportional loading, in 90 % of grains, dislocation cells are formed with clearly defined walls (Fig. 2.7b).

In the research described earlier in this chapter, Zhang and Jiang (2005) (cf. Fig. 2.3) also studied dislocation structures. It turns out that, in both types of loading, proportional and non-proportional, cellular dislocation structures appeared. However, the nature of these structures was different. The cells from non-proportional loading had thinner and denser walls, and their definition was greater. The sizes of the cells in non-proportional loading were smaller.

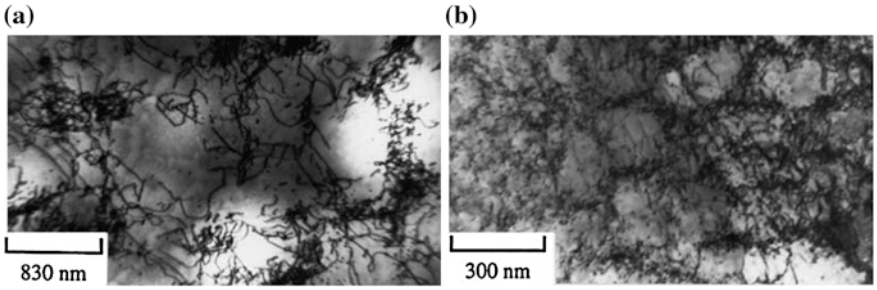

Fig. 2.7 Dislocation structures formed in the following conditions: **a** tension/compression and torsion, **b** non-proportional loading with "butterfly" loading path (Bocher et al. 2001)

The authors formulated a correlation between the amplitude of stress saturation and the size of the cell. The amplitude increases linearly (hardening is greater) with the inverse of the diameter of the cell.

To summarise the above research descriptions, one may venture to say that, in comparison to dislocations systems that occur in proportional loading, the non-proportional loading exhibits the following specific properties:

- Greater dislocation density,
- More uniform dislocation distribution,
- Smaller size cells,
- Greater disorientation of cells,
- Greater definition of dislocation in cell walls, and
- Dislocation remaining inside the cells.

Non-proportional dislocation structures are analogously related to proportional dislocation structures with a greater and lesser degree of failure (e.g. due to a larger number of cycles) in proportional loading. Some researchers (Rios et al. 1989; Xiao et al. 2000) emphasise that non-proportional dislocation structures are similar to dislocation structures achieved in proportional loading but with a sufficiently higher strain value. It is similar for the number of fatigue cycles. The differences between non-proportional and proportional dislocation structures are similar to the differences that occur between the structures formed after a greater number of cycles and the structures formed under a smaller number of cycles. The property that is specific only for non-proportional structures is the occurrence of dislocation inside the cells producing a more even distribution.

An analysis of non-proportional dislocation structures and their comparison with proportional structures leads to the conclusion that, for certain materials, non-proportional loading causes more damage than proportional loading. The influence of non-proportionality on the mechanism of dislocation evolution is the main cause of the decrease of fatigue strength and the reduction in the fatigue limit.

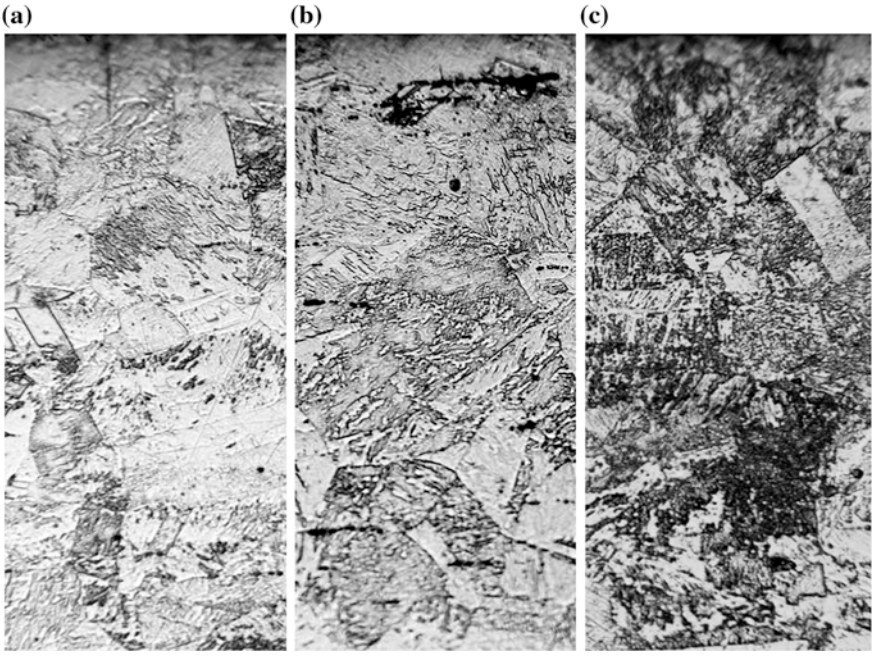

Fig. 2.8 Steel microstructure after fatigue trials: **a** tension, **b** torsion, **c** block loading (Skibicki and Dymski 2010)

2.1.3 Strain Induced Phase Transformations

There is also the influence of non-proportional loading on the course of structural changes induced by plastic strain. Skibicki and Dymski (2010) conducted microstructural comparative research on austenitic steel X5CrNi18-10 under proportional and non-proportional loading. In this study, the samples were subjected to three types of tests: tension-compression, torsion and block loading, and alternating tension-compression and torsion. The value of equivalent stress, according to Huber-von Mises, in all trials was the same. The alteration of the principal axes between blocks allows one to classify the third type as non-proportional. For the first two types of loading, the average life was at 20,000 cycles; however, in the third type, the life was much shorter, and was about 10,000 cycles.

The most interesting aspect of this study concerned phase transformations that took place during the experiment. The assumed cyclic loading value caused a martensitic transformation induced by plastic strain in the assessed areas of specimens in all types of loading. The microstructure of steel shows that the plastic strain induced transformation was the most intensive during block loading, that is, when fatigue loading produced changes in the principal (Fig. 2.8c). The specimens subjected to proportional loading produced less martensite and with a smaller number of grains (Fig. 2.8a, b).

2.2 Stress–Strain Relationships

2.2.1 Additional Cyclic Material Hardening

The materials under non-proportional loading which form dislocation structures described in Sect. 2.1.2 also have additional cyclic hardening. This effect may be illustrated by comparing cyclic strain curves for proportional and non-proportional loading (Fig. 2.9). Socie (1996) estimated that, for the austenitic steel he studied, the stress values for the hardening curve in sinusoidal loading, which is out-of-phase by 90 %, is twice as large as in proportional loading.

The results of studies conducted by Colak (2004) allow one to observe how the value of additional hardening is related to the degree of loading non-proportionality. For proportional loading (path 1, Fig. 2.10), the cyclic hardening curve stabilises at the level 200 MPa (Fig. 2.11), for paths of the highest degree of non-proportionality in the form of circle and square (paths 4 and 5, Fig. 2.10) the value of hardening is about 350 MPa (Fig. 2.11).

2.2.2 The Cross-Hardening

Block loading with different types of loading, e.g. bending and torsion blocks, can be also considered non-proportional loading. The blocks differ in the position of the principal axes; therefore, between the blocks, there is an abrupt change in the direction of the principal axes. The sequence of a different type of loading blocks causes the distinctive additional hardening called *cross hardening*.

Chen et al. (2006) analysed this type of hardening in the change of blocks from tension-compression to torsion. The material under investigation exhibited softening (Fig. 2.12a, b). The change of blocks to torsion was accompanied by cross hardening. If the change takes place after a 25 % life period, stress increases from 312 to 419 MPa (Fig. 2.12a), and if the change of blocks happens after 65 % of the trial duration, the stress changes from 334 to 455 MPa (Fig. 2.12b). Next, another cyclic softening of material is observed with a stability at 351 MPa in the first case and 406 MPa in the second. The hardening effect turns out to be longer lasting in the second case—the ratio between the amplitude of the saturation state from the second block to the saturation state amplitude in the first block is 1.13 in the first trial, and 1.22 in the second. This observation should be significant for formulation hypotheses of fatigue damage accumulation.

Shamsaei et al. (2010a) conducted an experiment that compares the value of additional cyclic hardening and cross hardening. In their experiment, trials were performed with sinusoidal proportional loading, sinusoidal non-proportional loading with a 90° phase shift, and two trials where the block loading consisted of proportional loading cycles with a guided change of the principal axes. The path marked FRI made fully reversed axial-torsion cycles with a gradually changing

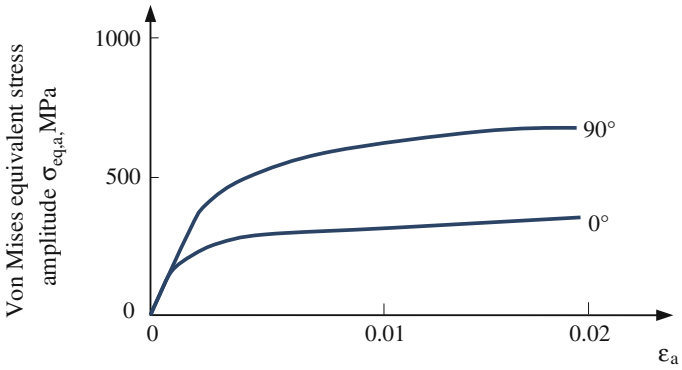

Fig. 2.9 Hardening curves for in-phase and out-of-phase loading for 304 (Socie 1996)

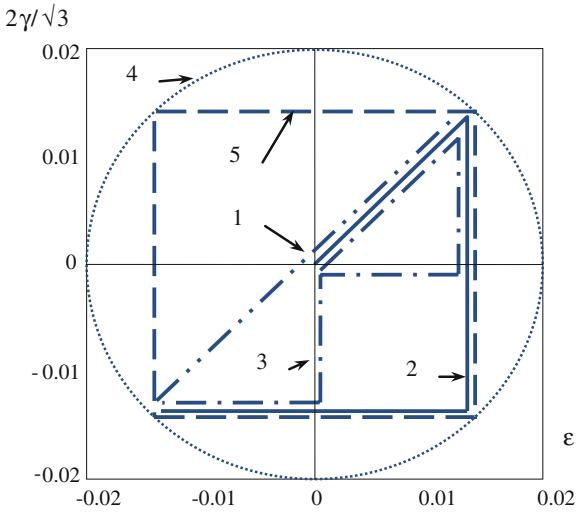

Fig. 2.10 Loading paths in the study (Colak 2004)

amplitude ratio between torsion and tension/compression in order to obtain a path rotation by 1° (Fig. 2.13a). The path marked FRR had the same proportional component cycles, but their realisation, due to the location of principal axes, was random (Fig. 2.13b).

For the non-proportional FRI and FRR paths, additional stress hardening was observed due to the interaction of the slip systems, because many slip systems were activated in various directions in those cases. However, there was a difference between the FRI and FRR path. For FRI, the change in strain direction was very "slow" which gradually activated the slip systems. The authors registered hardening values for FRI and FRR paths and compared them to the value for proportional loading and non-proportional loading with phase shift by 90°. The hardening for both FRI and FRR falls between proportional and non-proportional

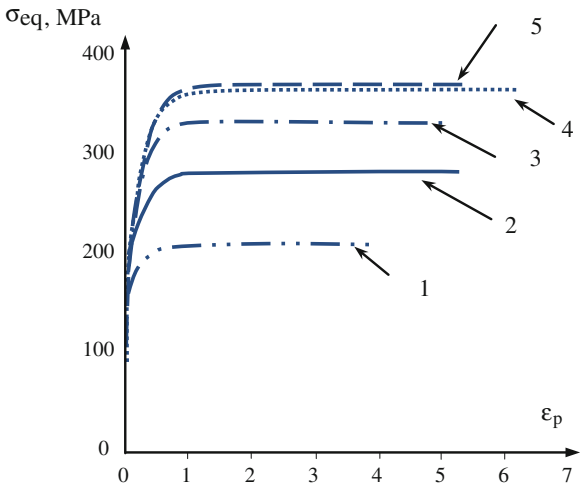

Fig. 2.11 Loading paths in the study (Colak 2004)

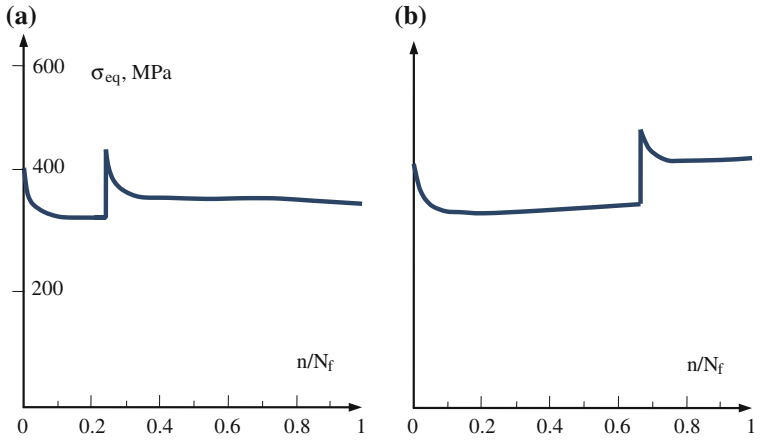

Fig. 2.12 Changes in the value of equivalent stress when changing from tension/compression to torsion after 25 % of life (**a**) and 65 % (**b**) of life (Chen et al. 2006)

loading (Fig. 2.14). However, the mode of activating the slip systems influences the hardening value. The "sudden" change in loading direction for FRR loading caused a higher cross-hardening value than the "slow" change for FRI loading.

Additional cyclic hardening and cross hardening are a result of the additional interaction of dislocation, which is evident in dislocation structures images, which takes place with the rotation of the principal axes. The existence of these phenomena indicates the intensification of the failure processes when the principal axes rotate.

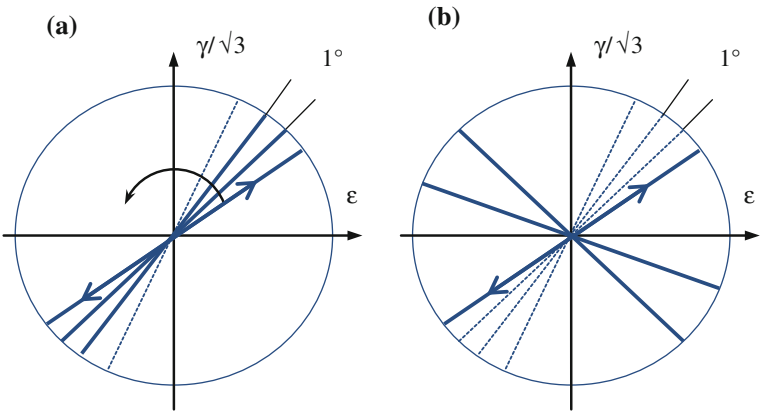

Fig. 2.13 Loading paths: **a** proportional fully-reversed axial-torsion cycles with 1° increments starting from the pure axial cycle FRI, **b** like FRI load path but the sequence of loading is random between 1° and 360° FRR (Shamsaei et al. 2010a)

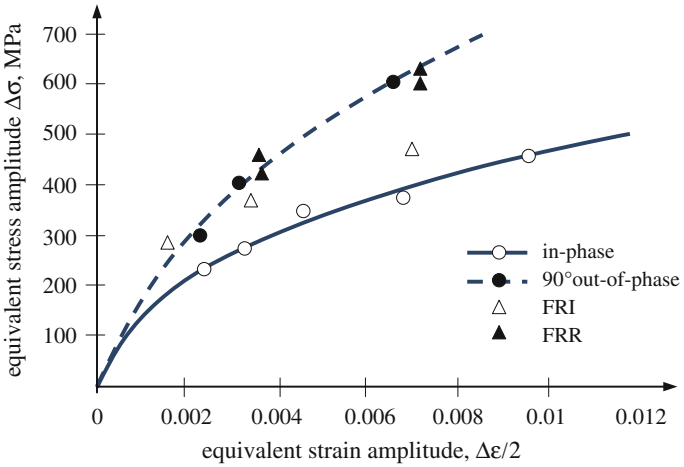

Fig. 2.14 Hardening values for proportional and non-proportional loading and for FRI and FRR (Shamsaei et al. 2010a)

2.2.3 Ratcheting

Non-proportional loading, moreover, influences the changes in the mean plastic strain accumulated during controlled periodic stress with a mean value.

Hassan et al. (2008) conducted research on this issue and analysed 5 types of loading paths (Fig. 2.15). In all analysed cases, the maximum equivalent stress and normal mean stress were naturally the same as follows: $\sigma_{eq} = 200$ MPa i

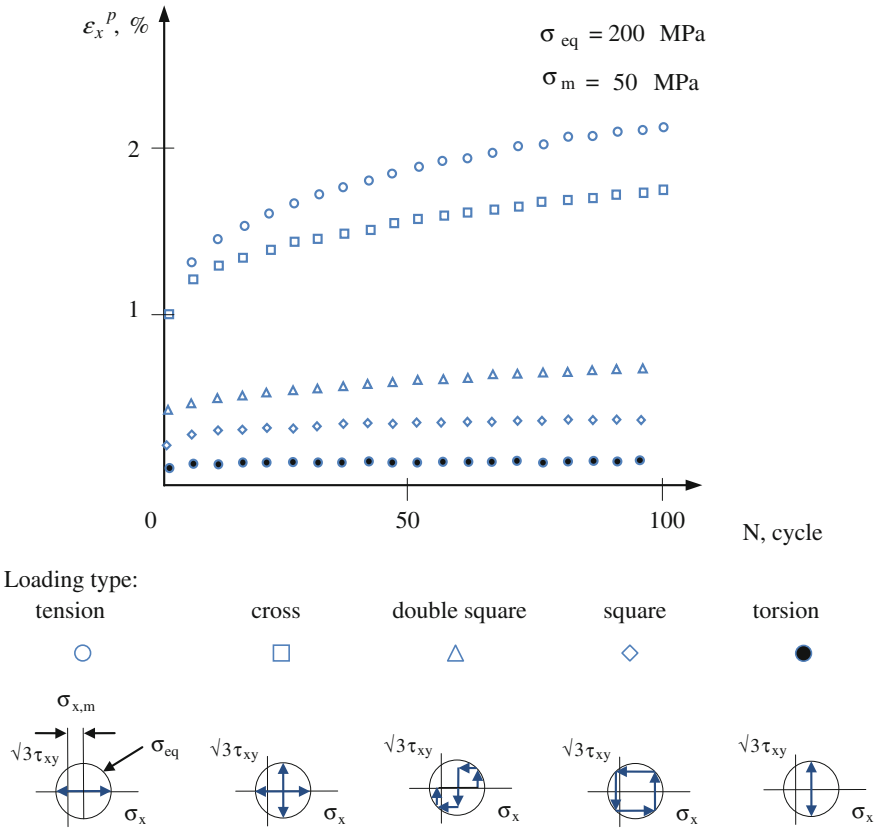

Fig. 2.15 The values of mean plastic strain for 5 loading cases with different degree of non-proportionality, the same values of equivalent stress, and mean normal stress (Hassan et al. 2008)

$\sigma_{x,m} = 50$ MPa. It turned out that the value of the cumulated plastic strain was smaller under non-proportional loading than in the tension-compression trial (Fig. 2.15). With an increase of non-proportionality, from "cross loading" (tension with torsion), through "double square," to the square shaped path, the *ratcheting* value kept decreasing, eventually taking on values comparable to those in torsion.

2.3 Thermal Effects

Formation of plastic strain is accompanied by temperature increase. Dependence between strain originating from different types of loading, including non-proportional, and temperature changed were studied by Lipski and Skibicki (2012).

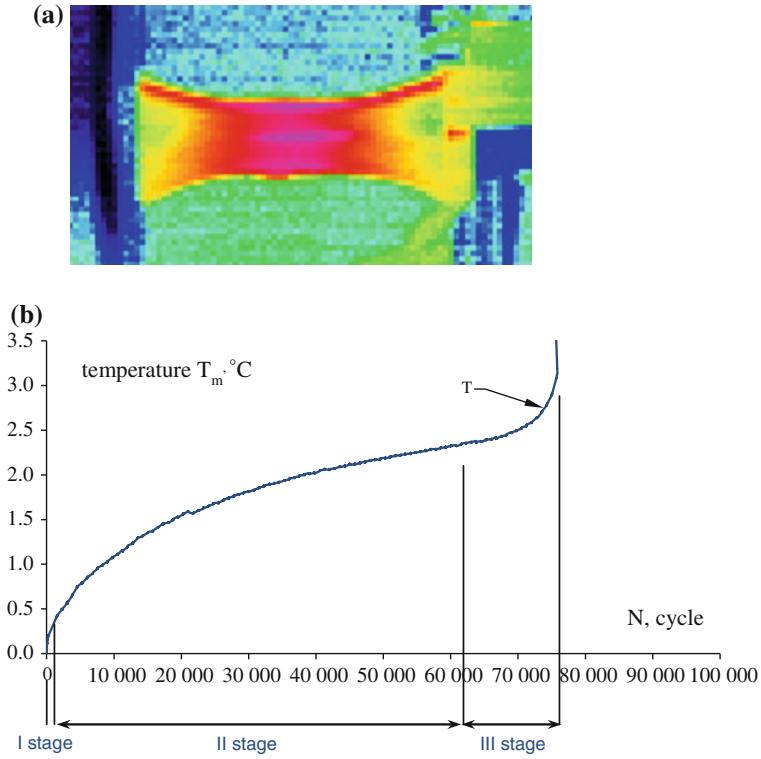

Fig. 2.16 Changes of average specimen surface temperature T_m

Figure 2.16 illustrates the temperature on the surface of the specimen, and Fig. 2.16b shows the curve of average temperature T_m during fatigue trial. Three characteristic stages may be distinguished in those curves:

- I—fast increase of the average temperature related to initial loading phase,
- II—stable increase of the average temperature of the specimen,
- III—fast increase of the average temperature related to final loading phase.

Figure 2.17a shows the temperature change graph for all fatigue types: tension-compression (TC), torsion (T), proportional loading (P), and two non-proportional loading trials differing in amplitude ratios (N5: $\lambda = \tau_a/\sigma_a = 0.5$ and N8: $\lambda = 0.8$).

The range of temperature changes during trials was the same—the specimen surface temperature changed from the loading start to the specimen failure by 2–3 °C. However, for non-proportional loading N5 and N8, the rate of temperature change turned out greater than for proportional and uniaxial trials; the same temperature increase was reached with a shorter life cycle, which is typical for non-proportional loading.

Figure 2.17b, c shows the change in plastic strain and dissipated energy as a result of plastic strain. The final energy and strain values turned out greater in

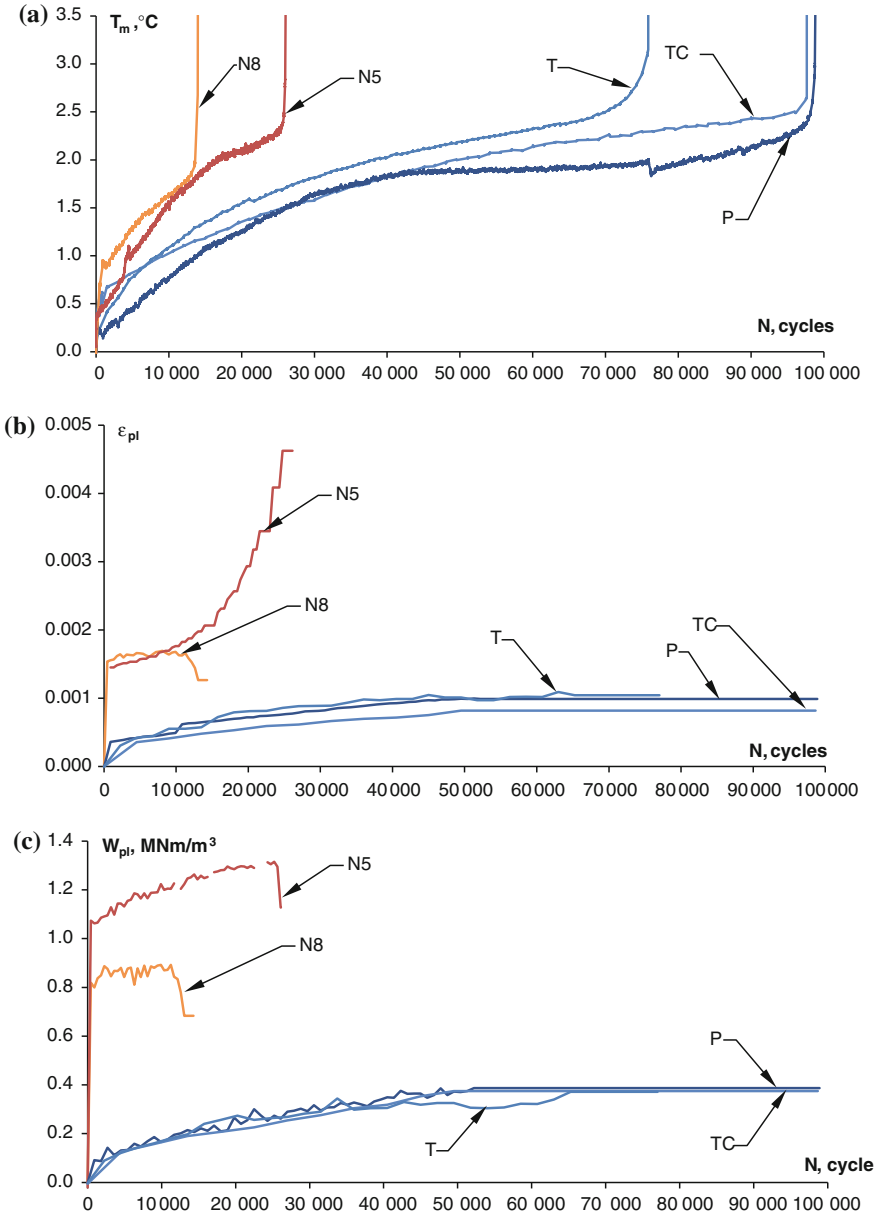

Fig. 2.17 Changes of average specimen surface temperature T_m recorded for individual loading types (**a**), changes of plastic strain ε_{pl} (**b**), and changes of plastic strain energy W_{pl} (**c**)

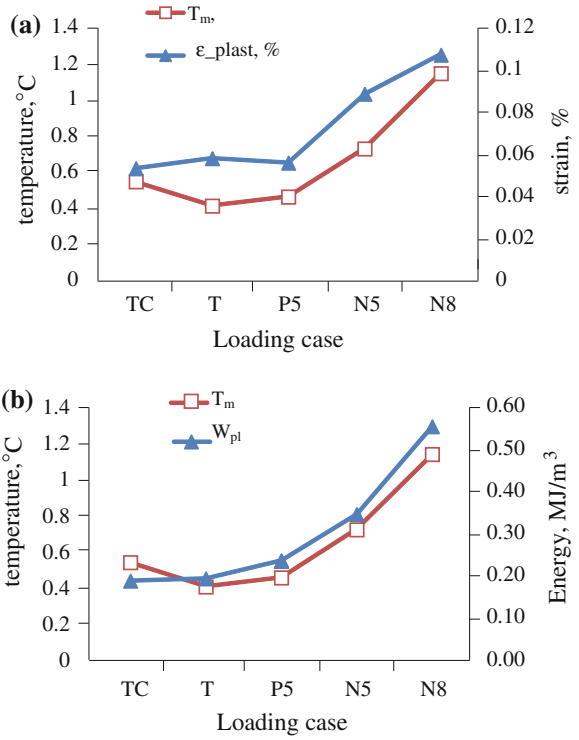

Fig. 2.18 Instantaneous values of temperature T_m compared to plastic strain ε_{pl} and plastic strain energy W_{pl}

non-proportional loading. They were accompanied by the same total temperature increase in all trials (2–3 °C).

Moreover, the relationships were compared for instantaneous temperature values, strain, and energy for proportional and non-proportional loading. These values were compared for different types of loading with an 8,000-cycle life. Figure 2.18a shows a comparison of mean temperature and plastic strain, and Fig. 2.18b shows mean temperature and plastic strain energy. The differences between different types of loading for each analysed value are similar in character. For non-proportional loading, they are greater than for proportional and uniaxial loading.

2.4 Fatigue Crack Growth

2.4.1 Initiation and Growth of Small Cracks

Studying the number and directions of fatigue micro-cracks provides important information about material failure in loading. It is estimated that the initiation and development of micro-cracks constitutes in many cases, about 90 %, of total fatigue life. This means that the mechanisms that condition this process determine

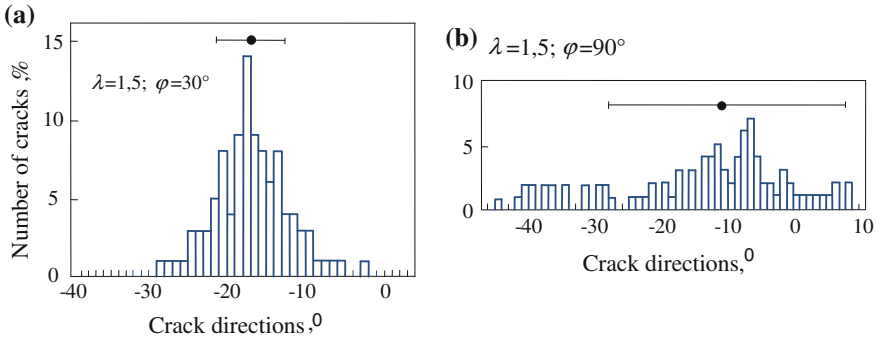

Fig. 2.19 The distribution of fatigue cracks directions for: **a** phase shift angle of 30° and **b** 90° (Kanazawa et al. 1977)

fatigue properties. Good understanding of these mechanisms and their inclusion in the parameters for calculation models may determine the accuracy of fatigue life estimates.

Kanazawa et al. (1977) studied crack distribution in 1 % CrMoV under sinusoidal loading where the amplitude ratio of shear stress to normal $\lambda = 1.5$ and phase shift angles are $\varphi = 0$, 30, 45, 90°. In all cases, the greatest number of cracks was initiated in the direction of the maximum shear stress. However, the distribution of crack directions was varied. With the increase of the phase shift angle, the standard deviation also increases taking a maximum value for the angle of $\varphi = 90^\circ$ (Fig. 2.19). This is because, with the increase of the phase shift angle, there is a greater number of directions are subjected to stress of a sufficient value for initiating crack growth. In Fig. 2.19a, one can notice that, for phase shift $\varphi = 30^\circ$, in angle range of -40 and $-30°$, the micro-cracks do not develop at all. In the most damaging instance, for phase angle of $\varphi = 90^\circ$, the stress of sufficiently large values for the initiation of micro-cracks appears in all directions (Fig. 2.19b).

Ohkawa et al. (1997) studied the distribution of fatigue crack directions for steel S45C for various λ ratios and φ angles of phase shift at various stages of fatigue process. During Stage I, after reaching 25 % of the life cycle, the length of cracks did not exceed 0.05 mm. Usually, the cracks developed in all directions, but the greatest number of cracks always fell in the direction of the maximum shear stress vector (Fig. 2.20a). The exception was one case, where $\lambda = 0.5$ and $\varphi = 90^\circ$, which has a uniform distribution of cracks that resulted from the uniform distribution of shear stress (Fig. 2.20b). For 95 % of fatigue life, the length of cracks was on average between 0.07 and 0.09 mm. The cracks then moved to Stage II, and, in the majority of the analysed cases, the greatest number of crack directions coincided with the direction of normal stress (Fig. 2.20c). Significantly, for $\lambda = 0.5$ and $\varphi = 90^\circ$, the distribution of the number of cracks remained uniform (Fig. 2.20d).

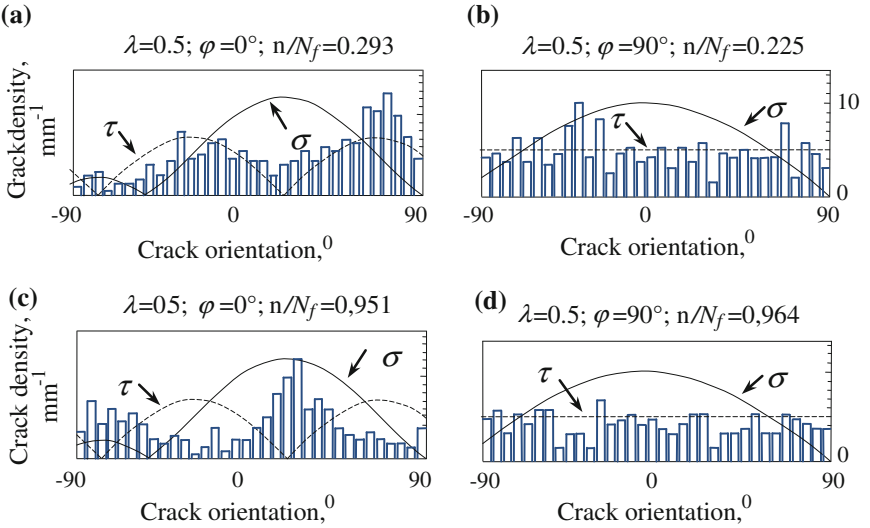

Fig. 2.20 The distribution of fatigue crack directions after **a**, **b** 25 % and **c**, **d** 95 % of life. The symbol σ indicates normal stress distribution, and τ indicates shear stress distribution (Ohkawa et al. 1997)

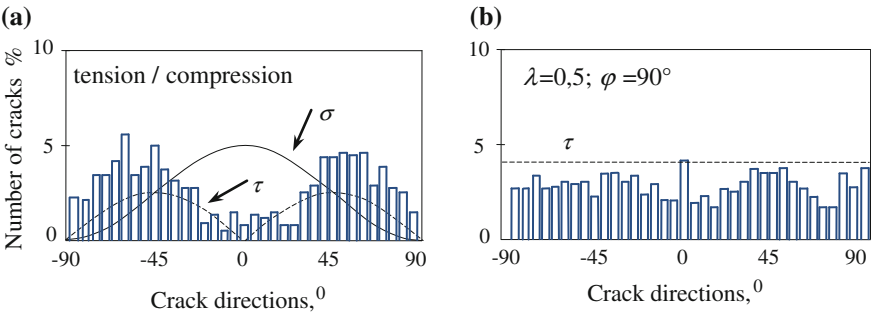

Fig. 2.21 The distributions of the number of fatigue micro-cracks (Ahmadi and Zenner 2005)

Ahmadi and Zenner (2005) conducted a study on the AlMgSi1 alloy. The results are very similar to those previously cited. The greatest numbers of cracks were in the directions of maximum shear. For example, Fig. 2.21a shows the distribution of the number of cracks for tension-compression. When the shear stress of the same values acts in all planes (for $\lambda = 0.5$ and $\varphi = 90^{\circ}$), the distribution of the number of cracks was also approximately uniform (Fig. 2.21b).

Verreman and Guo (2007) studies small cracks in steel 1045 under uniaxial proportional and non-proportional loadings. Complex states were obtained through axial and torsional loadings. The authors claim that microstructural small cracks always occurred at persistent slip bands for all loading cases. On the other hand,

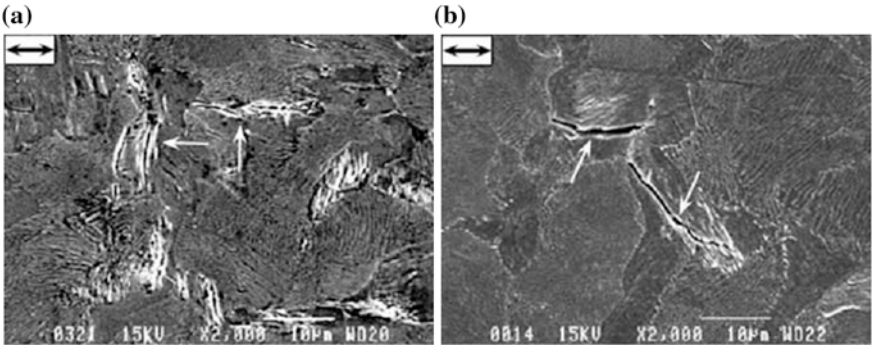

Fig. 2.22 Micro-structurally short cracks for out-of-phase loading: **a** $\lambda = 2$, **b** $\lambda = 0.5$ (Verreman and Guo 2007)

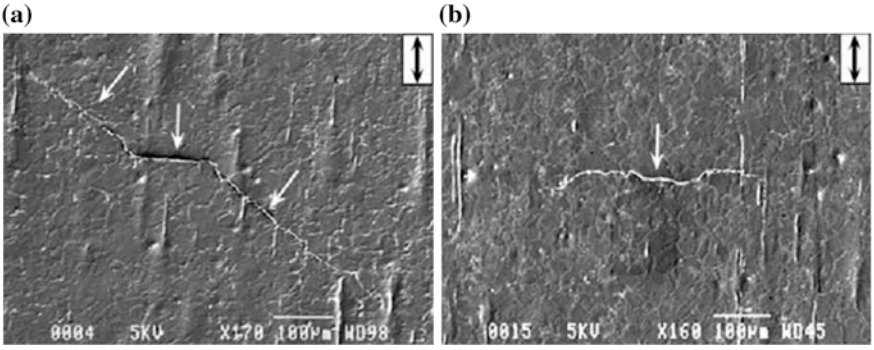

Fig. 2.23 Physically short cracks for out-of-phase loading: **a** $= 2$, **b** $\lambda = 0.5$ (Verreman and Guo 2007)

clearly, persistent slip bands, after several thousands of cycles, were oriented close to the maximum shear planes. There is no doubt about the relationship between the direction of the crack and the direction of the maximum shear stress in the case of uniaxial, proportional, and non-proportional stress for $\lambda = 2$ (Fig. 2.22a). Determining the directions for $\lambda = 0.5$ may turn out problematic, because the distribution of values is uniform for all angles. A sample photograph (Fig. 2.22b) shows that cracks are, in this case, positioned 0° and 45° angles to the axis of the specimen that is marked with a black arrow in the photograph.

In the same study, Verreman and Guo (2007) make very interesting observations concerning the development of the crack after Stage I. Physically, small crack growth depends on the type of loading. For a stress of $\lambda = 2$, during Stage I, the crack growth is similarly to that found under torsion, but with a difference. Out of the two planes of maximum shear stress, it propagates in the plane that is accompanied by the greater normal stress. This is the plane at 90° to the axis of the specimen (Fig. 2.23a). Next, during Stage II, it branches into a plane of maximum

normal stress amplitude. For a stress of $\lambda = 0.5$, because there is the same shear stress in all planes, the crack initiates in the plane of maximum normal stress (Fig. 2.23b). Further growth also occurs in the same plane, thus no crack branching is observed. According to the authors, the fact that both Stage I and Stage II run in the same material plane accounts for the more rapid crack growth and shorter life for $\lambda = 0.5$ loading.

The presented analysis of fatigue micro-crack distribution shows that, in relation to proportional stress, the rotation of the principal axes results in the accumulation of fatigue damage in a greater number of planes. In many cases, particularly for proportional stress, the maximum number of cracks appears in the direction of maximum shear stress. The greater the degree of non-proportionality, which is expressed in the cases with the value of phase shift angle and the stress amplitude ratio, the more uniform the crack distribution becomes. For the case with $\lambda = 0.5$ and $\varphi = 90^{\circ}$, where the distribution of shear stress is uniform, the further propagation of cracks is determined by normal stress.

2.4.2 Fatigue Propagation of Long Cracks

Qian and Fatemi (1996), based on an extensive publication review, claim that the number of studies concerning the inclusion of non-proportional stress in crack propagation models is very limited. At the same time, it should emphasised that there is a strong influence of non-proportionality on both the rate of propagation and on the direction of crack growth (Rozumek and Marciniak 2012).

Feng et al. (2006) analysed the influence of three types of loading in 1070 steel on crack propagation (Fig. 2.24). Loading I and II were proportional, while III, with a distinctive circular path, is included in non-proportional loading. The authors observed differences in the crack propagation concerning their shape as well as propagation rate. The crack developing under the influence the circular path of III had the greatest branching. The propagation rate was also the greatest for the crack developing under non-proportional loading (Fig. 2.25).

Crack propagation rate in Ti–6Al–4V was studied by Nakamura et al. (2011). According to them, fatigue cracks under non-proportional loading for a phase shift angle of 90° (marked as CP) propagated faster than those under proportional loading (Fig. 2.26). In this study, proportional loading investigations were conducted for push–pull loading (marked as PP) and torsion (marked as TP).

The rate of propagation for spatial loading was studied by Fremy et al. (2013), where the fastest development of cracks was observed for "Cube" type loading patch (Fig. 2.27). The potential difficulties in formulating a description of the behaviour of cracks under non-proportional loading resulting from the complexity of this phenomenon is evidenced in an attempt to compare the propagation rate for

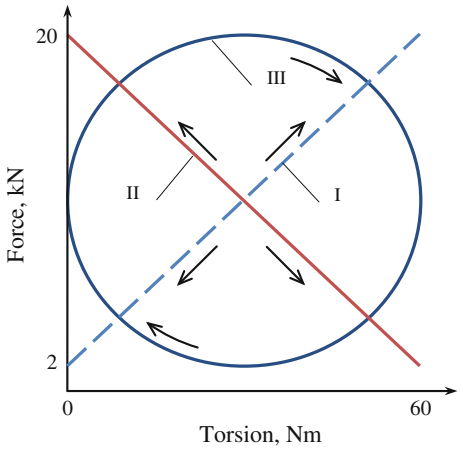

Fig. 2.24 Loading paths I, II, III in crack propagation rate study (Feng et al. 2006)

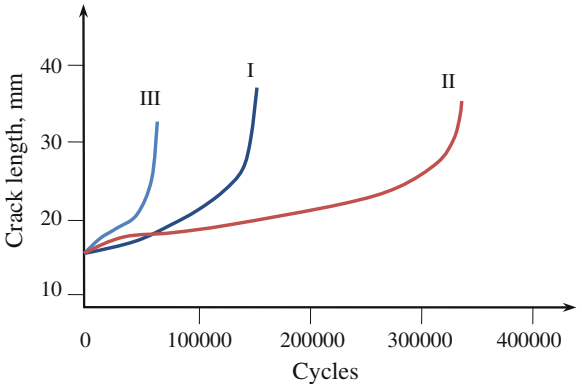

Fig. 2.25 Graphs for crack propagation length (Feng et al. 2006)

a proportional "Prop" path and "Star" type path. Even though the "Star" path can be classified as non-proportional, the crack caused by it develops slower than in the proportional path.

The influence of non-proportionality of loading on crack propagation results in difficulties in predicting the location of the fatigue fraction face. Carpinteri et al. (2002) presented a comparative compilation of several results of experimental studies and calculations by the tapering function method. The best predictions for the location of the fatigue fraction face are for proportional loadings, and they are worse for large values of phase shift angles between loading components $\pi/3$ and $\pi/2$ (Fig. 2.28).

According to Karolczuk (2006), the occurrence of such large errors in critical plane location prediction for non-proportional constant amplitude loading results from not taking into account plastic strains in calculation models.

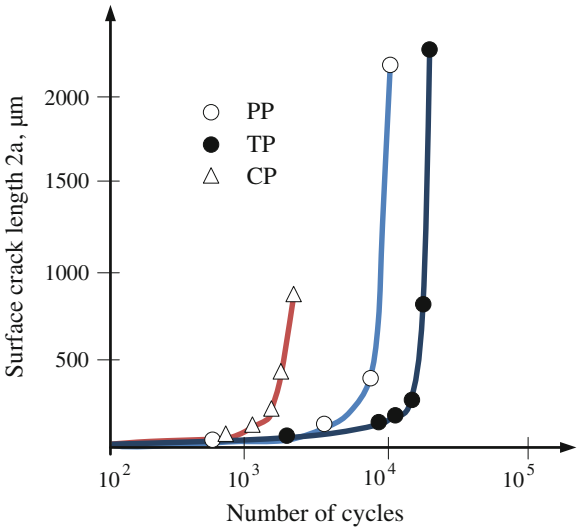

Fig. 2.26 Fatigue crack length for three types of loading paths (Nakamura et al. 2011)

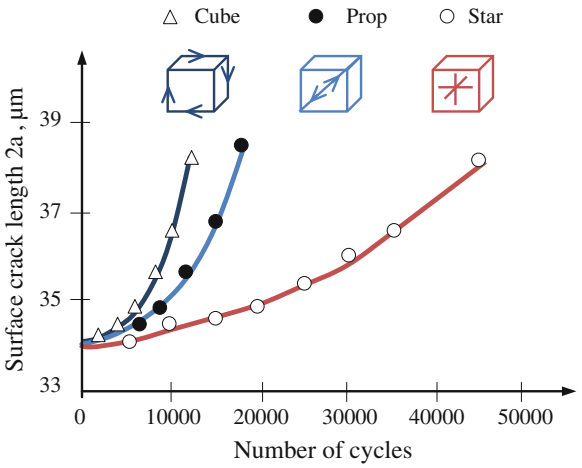

Fig. 2.27 Fatigue crack propagation for proportional and non-proportional loading paths, Fremy et al. (2013)

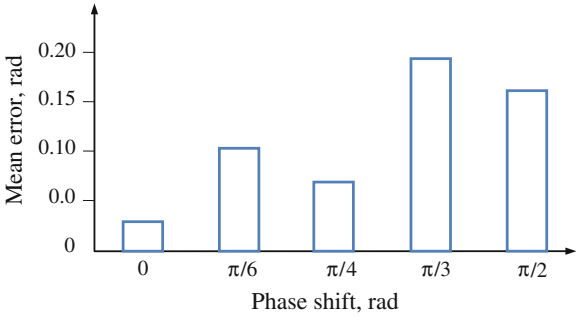

Fig. 2.28 Predicting error for the fatigue fracture faces as a function of phase shift (Carpinteri et al. 2002)

2.5 Influence on Fatigue Strength and Life

By influencing all the stages of the fatigue process, the non-proportionality of loading eventually leads to the change in fatigue strength and life in relation to that which emerges from the influence of proportional loading with identical equivalent stress or strain values.

In comparing fatigue strength and life in multiaxial fatigue, it is very important to decide which stress, strain or other values are being referred to. Comparing the strength between proportional and non-proportional loading for identical nominal loading values (amplitudes) usually leads to incorrect conclusions. An appropriate example will be given in Sect. 2.5.1 about the influence of non-proportionality on fatigue limit. Applying equivalent values for estimating non-proportionality is problematic, because it is difficult to estimate how much a given result reflects the actual influence of non-proportionality and how much it reflects the properties of a given damage model. The application of a given damage model to determine the effects of non-proportionality would require, first, to see whether this particular model accurately estimates fatigue properties in proportional loading and whether it takes into account non-proportionality in any way. It should be noted that, because of its properties, each criterion fulfilling these conditions (the choice of values describing the state of stress or strain, selection of their parameters), will present a different influence of non-proportionality (although it does not measure the influence of non-proportionality, it may react to such a state of stress or strain). This problem will be briefly discussed again in Sects. 2.5.1 and 2.5.2 concerning the influence of non-proportionality on fatigue life.

2.5.1 The Influence of Non-Proportionality on Fatigue Strength

One of the earlier studies on the influence of non-proportional loading on fatigue strength was conducted Nisihara and Kawamoto (1945). The authors studied the fatigue limit for three types of materials—hard steel, mild steel and cast iron (Fig. 2.29). In addition to the type of material, they included the degree of non-proportional loading in their study, which is a function of the phase shift angle between the components and the amplitude ratio of shear and normal stress.

It turned out that the influence of non-proportionality increased with the increase of the phase shift angle for all materials. However, the influence of λ turned out to be dependent on the type of material. Probably it could be correlated with the fatigue limit quotient for a given material. For mild steel, where the fatigue limit quotient of torsion to bending is $\tau_{-1}/\sigma_{-1} = 0.583$, the greatest change of fatigue limit in relations to proportional loading takes place with the amplitude ratio of $\lambda = 0.5$. For cast iron, where $\tau_{-1}/\sigma_{-1} = 0.949$, the greatest influence on the fatigue limit is for loading of $\lambda = 1.21$.

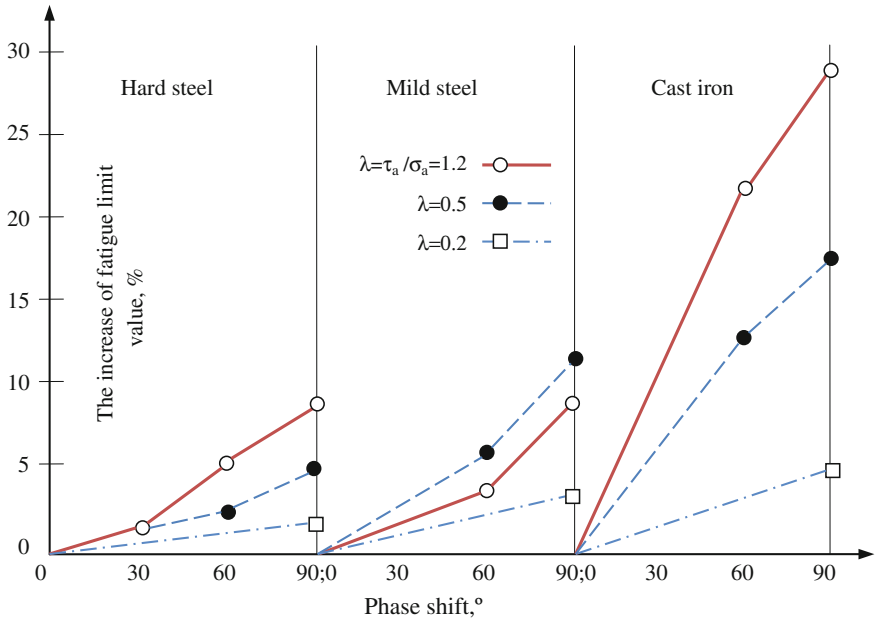

Fig. 2.29 The change of fatigue limit for various phase shifts in torsion and bending (Nisihara and Kawamoto 1945)

An analysis of the data in Fig. 2.29 shows that, in all cases with an increase of non-proportionality, there is an increase of fatigue limit. However, it should be remembered that the data analysed by Nisihara and Kawamoto refer to nominal stress amplitudes. In one study, Little (1969) showed that the increase of nominal stress, although useful in practical application, can be misleading when drawing general conclusions. If the maximum shear stress value is considered, instead of normal amplitudes, the decrease in fatigue life becomes evident. For the loading example of $\varphi = 0°$, $\sigma_x = 245.3$ MPa, $\tau_{xy} = 122.7$ MPa, the maximum shear stress has the value of 173.5 MPa, while for $\varphi = 90°$, $\sigma_x = 258$ MPa, $\tau_{xy} = 129$ MPa it is 129 MPa. The nominal value of shear stress thus increases from 122.7 to 129 MPa, while the maximum value of stress decreases from 173.5 to 129 MPa. This can be seen on the rotational transformation graphs for stress (Fig. 2.30), where the nominal value is on the X-axis. The maximum stress value marked on Fig. 2.30a with an arrow may not correspond to it.

Based on a similar data analysis of Nisihara and Kawamoto, Mcdiarmid (1986) showed that, for hard steel and mild steel, there is a decrease in the fatigue limit. A maximum drop in fatigue limit reached 25 %, while an increase in the fatigue limit was only found in cast iron. This is a very interesting example of the influence of non-proportionality, because it shows that this influence is not always unequivocally negative; it does not always lead to the loss of fatigue properties.

The influence of the phase shift angle was presented by Papadopoulos et al. (1997) who analysed the error in the application of various damage models for

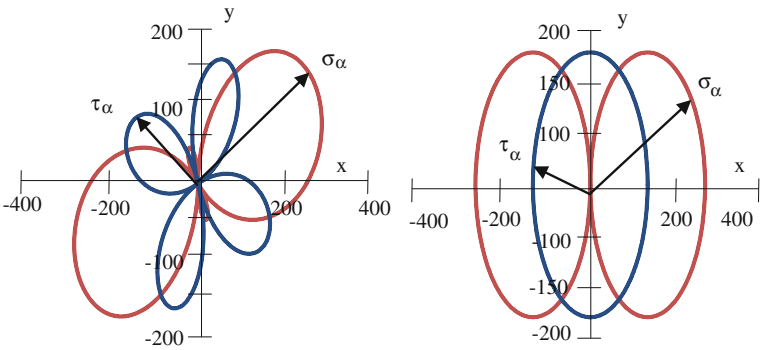

Fig. 2.30 Normal stress (*dotted line*) and shear stress (*continuous line*) distribution **a** $\varphi = 0°$, $\sigma_x = 245.3$ MPa, $\tau_{xy} = 127$ MPa, **b** $\varphi = 90°$, $\sigma_x = 258$ MPa, $\tau_{xy} = 129$ MPa. Data from the experiment for hard steel (Nisihara and Kawamoto 1945)

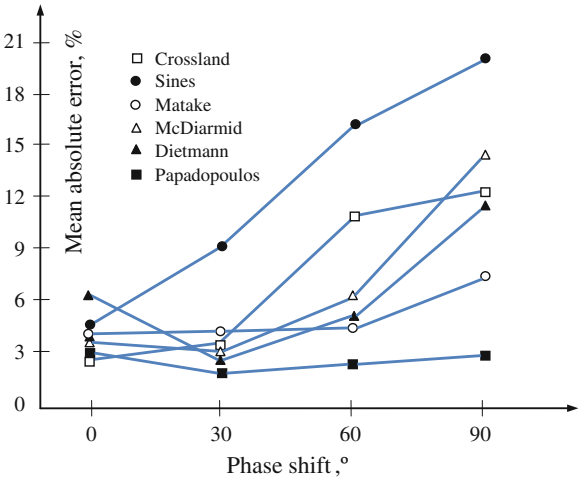

Fig. 2.31 Mean absolute error for fatigue limit prediction for different fatigue criteria (Papadopoulos et al. 1997)

proportional loading for estimating the fatigue limit in bending and torsion with a phase shift of the components. This analysis was conducted for 43 items of experimental data from various publications. A majority of the models analysed are not able to accurately estimate the changes in the fatigue limit; therefore, the calculation error increases with the increase of non-proportionality reaching as much as 20 % of its value (Fig. 2.31).

Naturally, in such a case, it is difficult to show clearly the influence of non-proportionality, because it is not obvious to what extent the errors are part of a given calculation model. In order to accurately calculate the influence of non-proportionality, we would need a criterion that works accurately in the range of proportionality and does not take into account the non-proportionality of loading in any way.

2.5.2 The Influence of Non-Proportionality on Fatigue Life

The effect of non-proportionality on fatigue life depends on the degree of the non-proportionality of loading. For sinusoidal loadings, this degree is expressed by the angle of the phase shift between the components and the ration of the component amplitudes.

The influence of the phase shift angle for 304 steel, depending on the property describing the loading, was presented by Li et al. (2011). It appears that the influence of the non-proportionality of loading "depends" on the choice of the quantity to describe the state of stress or strain; however, it can be generally stated that, the greater the value of the phase shift, the smaller is the value of fatigue life (Fig. 2.32).

The influence of non-proportionality controlled by the value of component amplitudes was studies by Skibicki et al. (2012). The fatigue life graphs in Figs. 2.33 and 2.34 indicate the results of experimental studies for X2CrNiMo17-2-2 and copper Cu-ETP. They were subjected to tension-compression (TC), torsion (T), complex proportional loadings (P#), and non-proportional loadings with a component phase shift equal to 90° (N#). The number in the (#) symbol indicates the quotient of the amplitudes of stresses multiplied by 10, i.e. $\tau_{xy}/\sigma_x * 10$.

The graphs correspond to tension-compression (TC), torsion (T), and proportional trial (P), after applying the criterion by Zenner et al. (2000). (These results are marked with squares in Figs. 2.33 and 2.34). The results fall within the scatter band of factor 2 for both materials (Figs. 2.35 and 2.36). The graphs for non-proportional trials fall within the smaller life-cycle values (these results are marked with circles in Figs. 2.33 and 2.34) and go beyond the scatter band of factor 3 (Figs. 2.35 and 2.36), defined as follows:

$$scatter\,band = \max \begin{cases} \frac{N_{cal}}{N_{exp}} & \text{for } N_{cal} > N_{exp} \\ \frac{N_{exp}}{N_{cal}} & \text{for } N_{exp} > N_{cal} \end{cases} \tag{2.1}$$

where N_{cal} is the calculated (predicted) fatigue life and N_{exp} is the experimental (observed) life.

It turns out that, the closer the value of the amplitudes quotient is to the fatigue limit quotient t_{-1}/b_{-1}, the more damaging the loading is. Figure 2.37 shows fatigue life values from graphs in Figs. 2.33 and 2.34 at the level of 310 MPa for X2CrNiMo17-2-2 and 170 MPa for Cu-ETP. The minima of fatigue life correspond to values that are approximate to the quotients of fatigue limits t_{-1}/b_{-1} of those materials.

The influence of the non-proportionality of loading on the fatigue life of metals often depends on the level of loadings. This effect is related to plastic strain—the higher the loading level, the greater the contribution of plastic strain, thus the stronger the effect of non-proportionality. (The mechanism of non-proportional loading will be discussed in Chap. 3 in detail.) This influence asymptotically decrease with a decrease in loading (Ellyin et al. 1991).

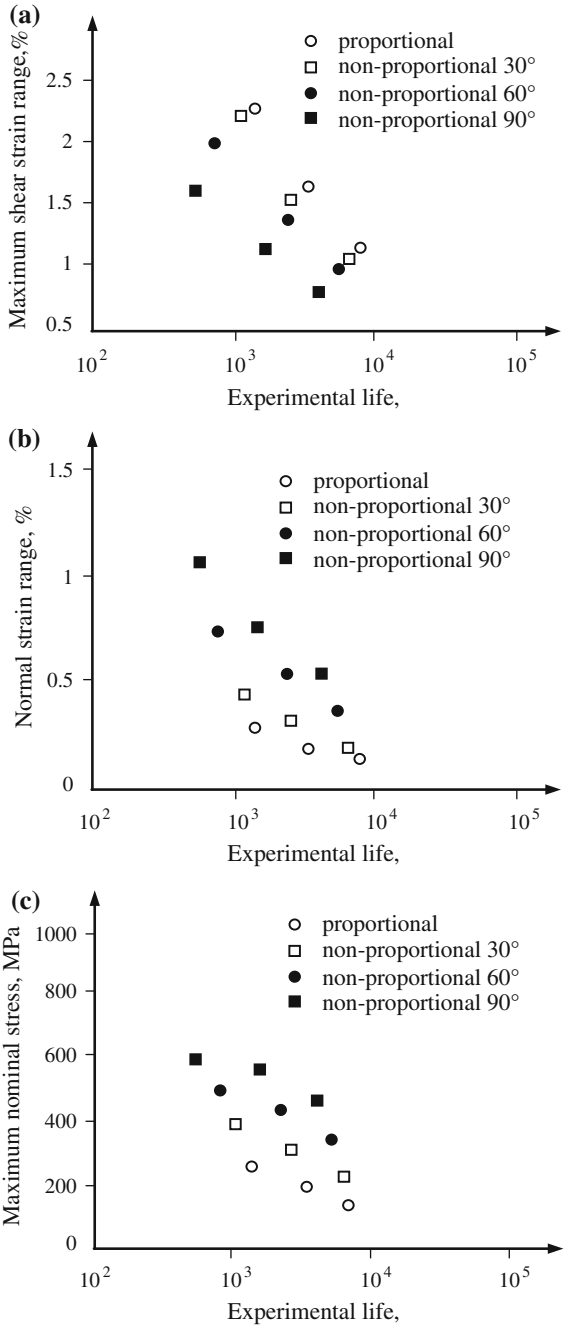

Fig. 2.32 The influence of the phase shift on fatigue life for different loading properties: **a** maximum shear strain range, **b** normal strain range, **c** maximum normal stress, (Li et al. 2011)

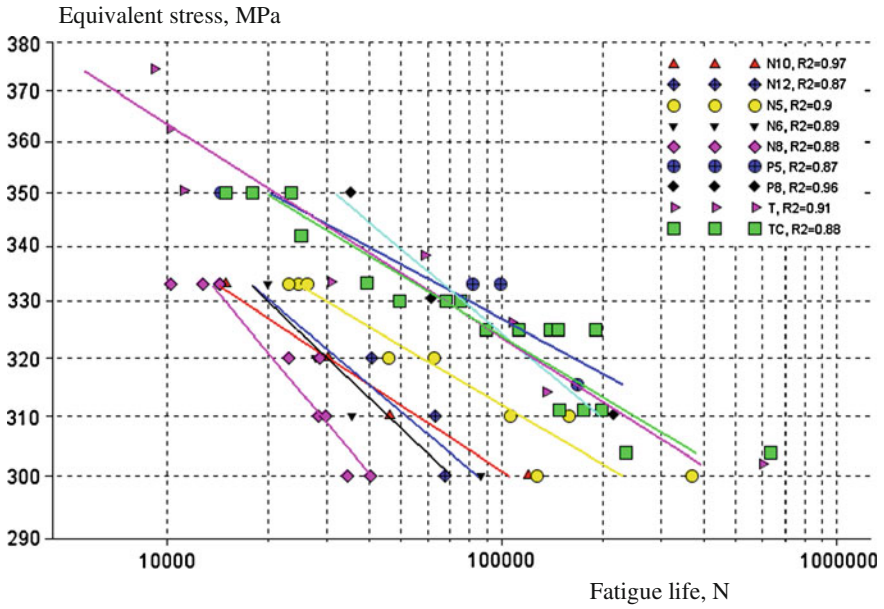

Fig. 2.33 The influence of the loading amplitude quotient of components on fatigue life for X2CrNiMo17-2-2 steel

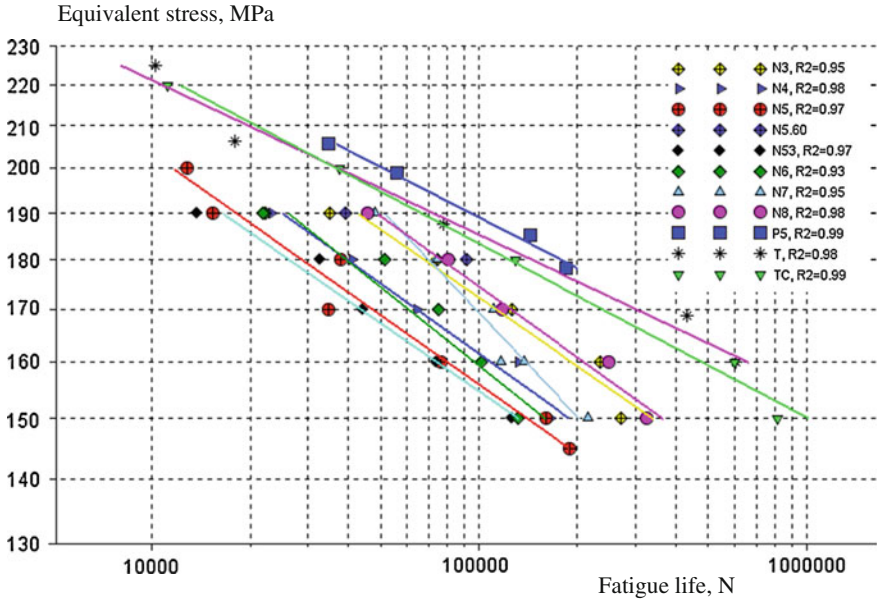

Fig. 2.34 The influence of the loading amplitude quotient of components on fatigue life for Cu-ETP copper

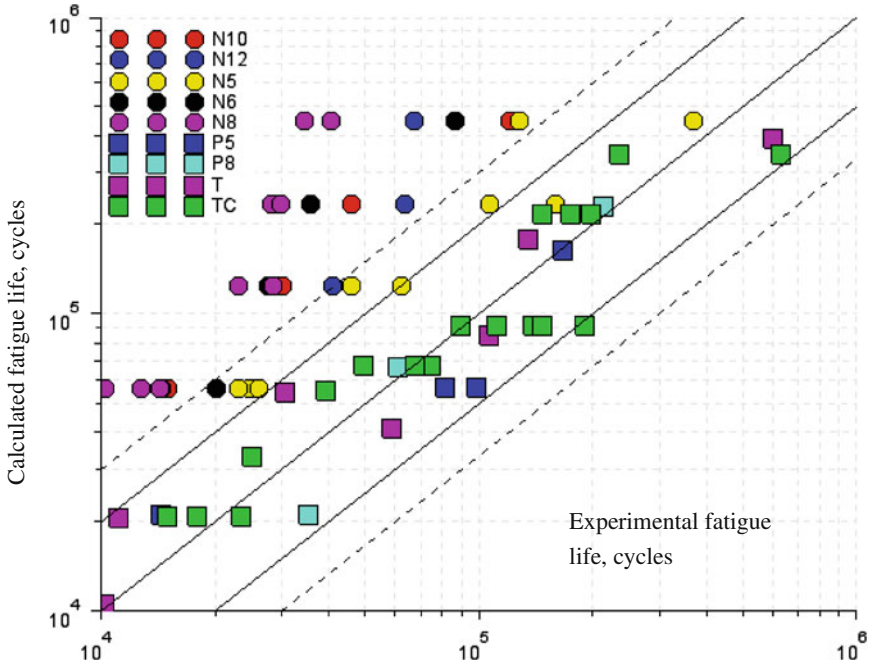

Fig. 2.35 A comparison of experimental and calculated life for X2CrNiMo17-2-2

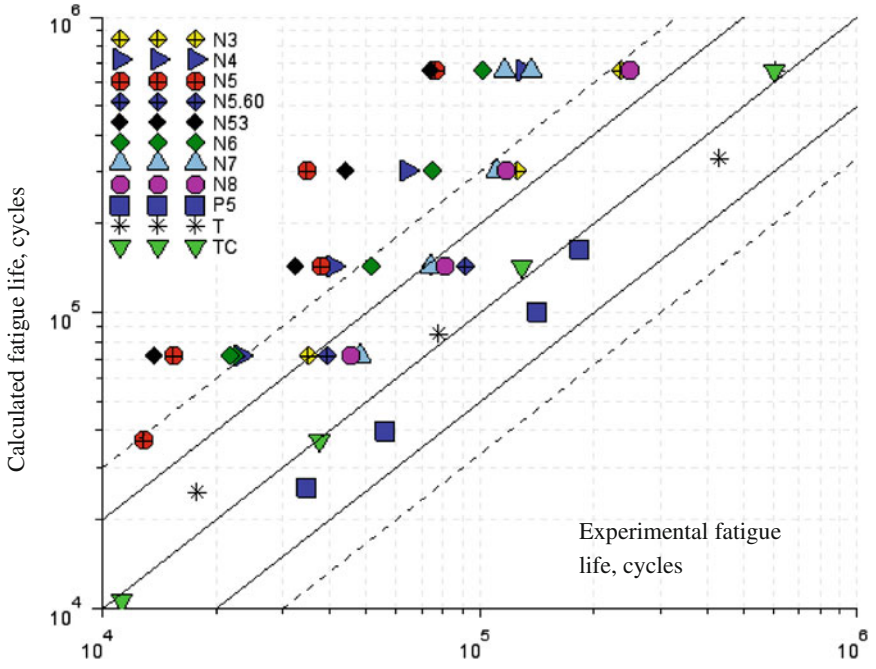

Fig. 2.36 A comparison of experimental and calculated life for Cu-ETP

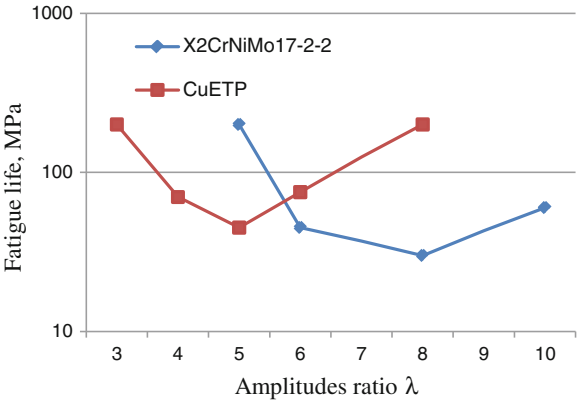

Fig. 2.37 The influence of the amplitudes of loading components λ on fatigue life

Table 2.1 Comparison of fatigue life for proportional and non-proportional loadings for different levels of stress and the same level of non-proportionality of load

Material and source	σ_{xa} (MPa)	Mean fatigue life		Decrease in fatigue life (%)
		Proportional loading	Non-proportional loading	
Ck45 (Simburger 1975)	190	313,457	97,284	69
	230	50,565	12,291	76
	270	8,157	1,553	81
StE 460 (Sonsino 1983)	80	2,212,031	1,031,548	53
	120	447,373	143,374	68
	160	90,479	19,927	78

The relationship between the level of stress and the influence of the non-proportionality of loading on fatigue life can be demonstrated using the examples of results in a studies on fatigue life in bending with torsion conducted by Simburger (1975) for Ck45 steel and Sonsino (1983) for StE 460. We can use these studies, because the stress amplitude ratios and the phase shift angle for the entire series of studies are the same, which is σ_{xa}. The percentage of the decrease in fatigue life for non-proportional loading in relation to proportional loading, for the three levels of stress, increases in both cases with the increase of stress, Table 2.1.

2.5.3 Block Loadings

Section 2.2.2 contains a description of cross hardening, which occurs between loading blocks that differ in the position of principal axes. A sequence of such

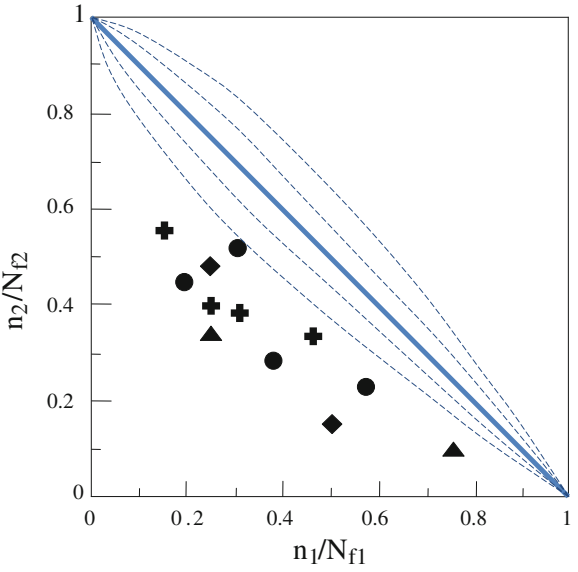

Fig. 2.38 The results of experimental studies for the following loading sequences: axial-torsion *rhombus*; proportional–non-proportional *circle*; non-proportional–proportional *cross*; torsion-axial *triangle*. Fatigue predicted with the linear damage hypothesis is marked with a *continuous line*, and damage curves based hypothesis are marked with *dotted lines* (Chen et al. 2006)

loading blocks has an effect on fatigue life that is similar to the phase shift for sinusoidal alternating loadings. For fatigue sensitive materials, fatigue life decreases under these loadings, which causes problems with predicting fatigue life through the hypotheses of fatigue damage accumulation known for the area of uniaxial loadings.

Chen et al. (2006) studied the possibility of describing fatigue failure accumulation in sequential loading—torsion-tension and tension-torsion—with the help of several models for fatigue damage accumulation, which include linear, double linear, damage curve based, and plastic interaction based as proposed by Morrow. None of the methods applied allowed an accurate description of fatigue behaviours. In Fig. 2.38, the experimental results are marked with geometric shapes. The influence of loading non-proportionality was so large that all the symbols fall outside the area delimited by the tested hypotheses.

Bonacuse and Kalluri (2003) studied the influence of sequences for axial and torsion loadings. They concluded that, for this type of loading, neither the Palmgren-Miner linear hypotheses for fatigue damage summation, nor the non-linear Manson hypothesis for damage curves could be applied. Based on this, the authors concluded that the character of the fatigue damage accumulation process of the studied loading sequence is different from when subjected to proportional loading.

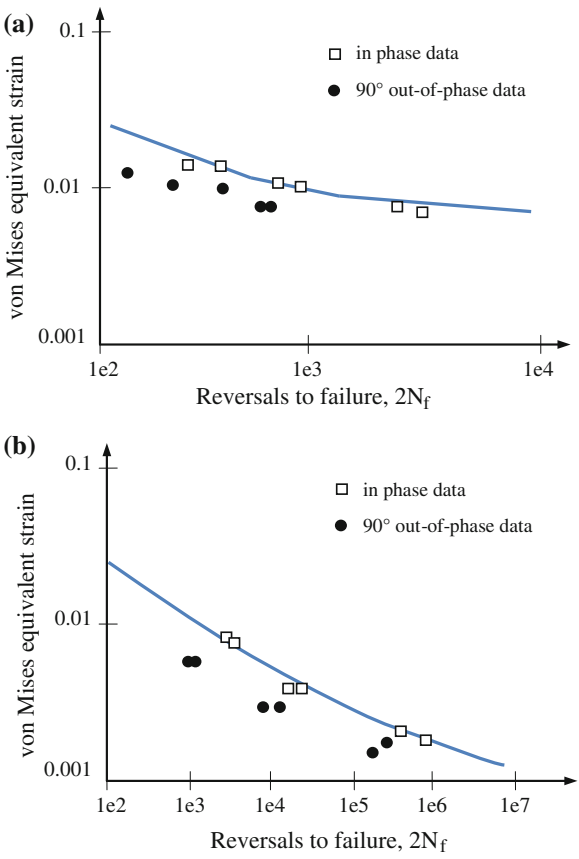

Fig. 2.39 Fatigue life graphs for proportional and non-proportional loadings for **a** Ti-6.5Al-3.4Mo steel, **b** 1050 N (Fatemi and Shamsaei 2011)

2.5.4 The Influence of Non-Proportionality on Materials Not-Exhibiting Additional Hardening

When analysing the influence of non-proportionality on fatigue life, the results for materials exhibiting additional cyclic hardening are often employed. For these materials, the influence of non-proportionality is beyond any doubt, and it is easy to demonstrate. It is considered that the influence of loading non-proportionality is tied to the intensification of dislocation processes manifesting in additional hardening of material. This problem will be discussed in more detail in Chap. 3.

However, Fatemi and Shamsaei (2011) present examples of studies on materials that do not exhibit (or exhibit only a small degree) additional cyclic hardening, but nonetheless, they are sensitive to the influence of non-proportionality. These studies include the study by Shamsaei et al. (2010b) shown in Fig. 2.39a or Shamsaei and Fatemi (2009) illustrated in Fig. 2.39b. In both cases, lower fatigue life is noticeable for non-proportional loadings. The loss of fatigue life is often

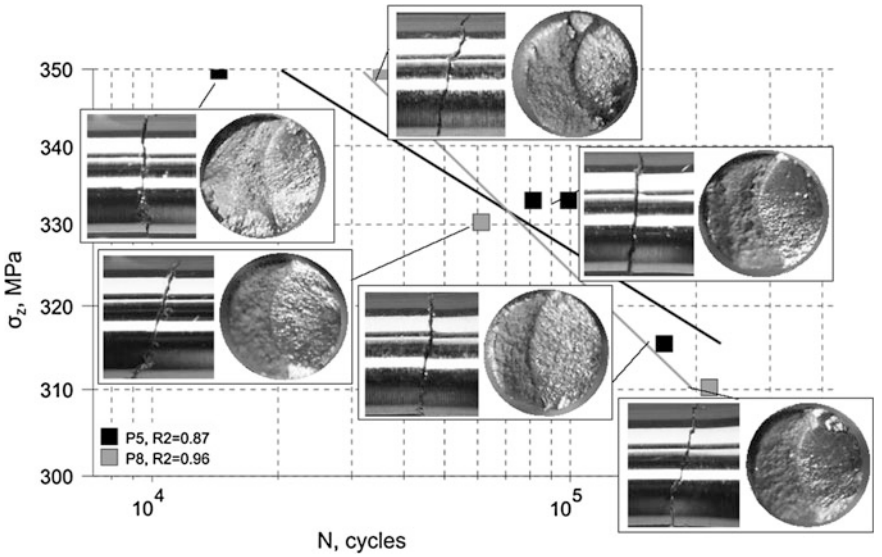

Fig. 2.40 Fractography of X2CrNiMo17-12-2 samples for proportional loading for $= 0.5$ and $\lambda = 0.8$

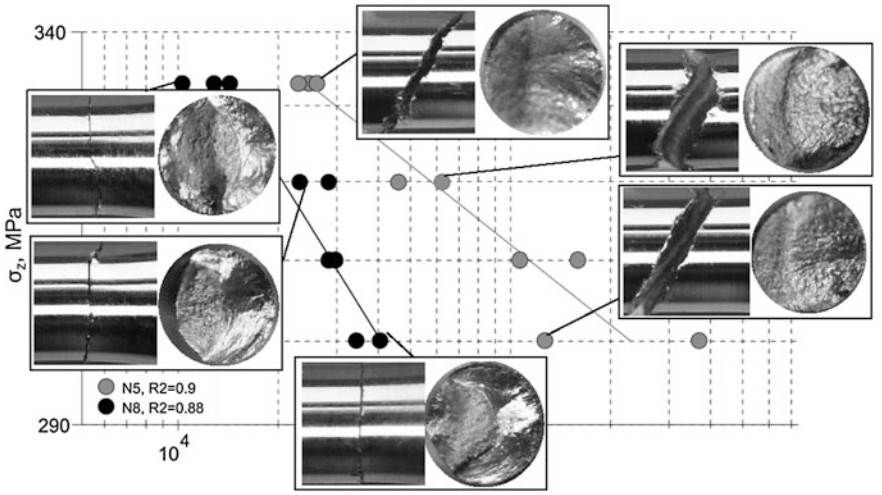

Fig. 2.41 Fractography of X2CrNiMo17-12-2 specimens for non-proportional loads for $\lambda = 0.5$ and $\lambda = 0.8$

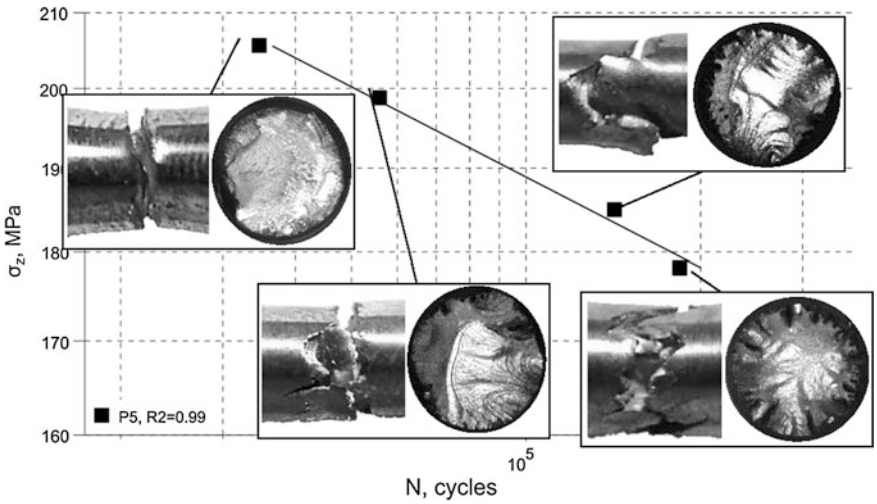

Fig. 2.42 Fractography of Cu-ETP samples in proportional loading for $\lambda = 0.5$

considerable, e.g., for 1050 N steel, the order of magnitude at 0.07 of equivalent von Mises strain (Fig. 2.39b). Moreover, Fig. 2.39b does not indicate any decrease in the influence of non-proportionality on fatigue life with a decrease in loading level.

These two observations can be only explained if we assume that, in this case, the role of dislocation mechanisms responsible for the existence of additional hardening in non-proportional hardening is insignificant. This problem will be further discussed in Chap. 3.

2.6 Macrostructure of the Material

The specimens in Sect. 2.5.2 (Skibicki et al. 2012) were additionally analysed fractographically. The authors conducted a comparative analysis of fatigue fracture faces from proportional and non-proportional trials.

Figure 2.40 shows fatigue fracture faces and fractures in specimens of X2CrNiMo17-12-2 under proportional loading, where the value of the coefficient was $\lambda = 0.5$ and 0.8. When the stress amplitude quotient was $\lambda = 0.5$, macrocracks propagated at a 7° angle, while for $\lambda = 0.8$, they propagated at 15°. The difference is 8°, and it is the same as the change in the value of the angle of principal axes. The fracture faces are similar to tension-compression faces. In the fatigue area, there are neither progression marks nor ratchet marks, and the initiation of fracture had one origin, which is a fast fracture zone decreased along with the decrease in loading. The only difference in relation to the fraction faces in

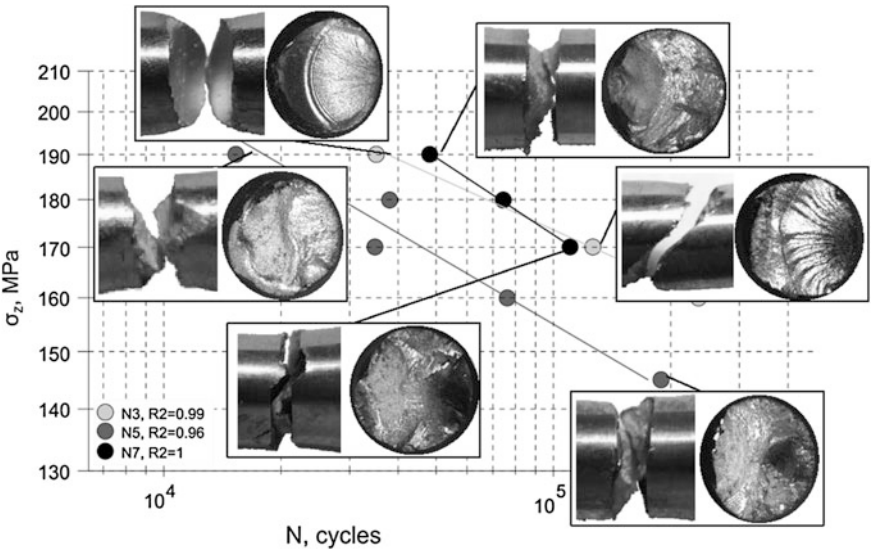

Fig. 2.43 Fractography of Cu-ETP samples in non-proportional loading for $\lambda = 0.3$, $\lambda = 0.5$, $\lambda = 0.7$

the uniaxial trial consisted in the crack developing more inwards [Case B (Socie and Marquis 2000)] than in the direction of the crack length.

Figure 2.41 shows faces and fractures of the X2CrNiMo17-12-2 specimens subjected to non-proportional loadings, with the coefficient $\lambda = 0.5$ and 0.8. For $\lambda = 0.5$, the macrocrack propagated at a 30° angle to the specimen's axis. The direction of the macro-plane of the fracture corresponds to the direction of the equivalent stress according to Huber von Mises. For a loading of $\lambda = 0.5$, the crack propagated more inwardly (Case B) than for $\lambda = 0.8$, where the larger share of torsion caused it to develop much more in the direction of the crack (Case A). The non-proportionality of loading caused the surface and edges of the crack to become very irregular, which means that the crack propagated in multiple planes.

Figure 2.42 shows the photographs of fracture faces and cracks of Cu-ETP specimens subjected to proportional loading with a $\lambda = 0.5$ coefficient. The fracture face for the specimen with the greatest loading resembles that of tension-compression with a low stress value, because there are no ratchet marks and multiple origins, and the fast fracture zone is relatively small. It can be observed that the crack developed as in Case A and to a larger extent than in the case of pure torsion. The lower the levels of loading, the more origin and ratchet marks appear. The walls of ratchet marks are slanted and tapered, which indicates the involvement of torsion.

Figure 2.43 contains a set of photographs of fracture faces and cracks in specimens made of Cu-ETP, which were produced in non-proportional loading with three different values of the λ coefficient. For $\lambda = 0.3$, the fracture face of the

specimen with the largest loading looks like the one for the tension-compression specimen. This is understandable, since the share of torsion is small. There are no ratchet marks, and there are several progression marks in the proximity of the remnant zone. The plane of the macro-crack is perpendicular to the axis of the specimen. On the fracture face of the specimen subjected to smaller loading, numerous river marks are visible with ends indicating that the fracture grew in many directions. The plane of the macro-crack is at a 45° angle to the axis of the specimen. For $\lambda = 0.5$, the fatigue fracture face of the specimen subjected to the greatest loading has a large remnant zone, which means the material was considerably strained. The fatigue zone is irregular, and the crack developed from many loci and in various planes. For the specimen subjected to loading of the lowest value, the remnant zone is smaller, and the fatigue zone as well as the macro-crack indicates that the crack propagated in many planes. Predominance in propagation of Type A cracks is visible. The macro-crack of the specimen subjected to non-proportional loading with a highest value coefficient of $\lambda = 0.7$ is perpendicular to the axis of the specimen. The predominance of an A-type crack is considerable, and the surface of the fracture face bears marks of friction. The macro-crack and the fatigue fracture face indicate crack initiation in several loci and growth in a larger number of planes.

References

Ahmadi A, Zenner H (2005) Simulation of microcrack growth for different load sequences and comparison with experimental results. Int J Fatigue 27(8):853–861. doi:10.1016/j.ijfatigue.2005.02.005

Bocher L, Delobelle P, Robinet P, Feaugas X (2001) Mechanical and microstructural investigations of an austenitic stainless steel under non-proportional loadings in tension-torsion-internal and external pressure. Int J Plast 17(11):1491–1530. doi:10.1016/S0749-6419(01)00013-4

Bonacuse PJ, Kalluri S (2003) Axial and torsional load-type sequencing in cumulative fatigue: low amplitude followed by high amplitude loading. In: Biaxial/Multiaxial fatigue and fracture. ESIS Publication 31. Elsevier, Amsterdam

Carpinteri A, Karolczuk A, Macha E, Vantadori S (2002) Expected position of the fatigue fracture plane by using the weighted mean principal Euler angles. Int J Fract 115(1):87–99. doi:10.1023/A:1015737800962

Chen X, Jin D, Kim KS (2006) Fatigue life prediction of type 304 stainless steel under sequential biaxial loading. Int J Fatigue 28(3):289–299. doi:10.1016/j.ijfatigue.2005.05.003

Colak OU (2004) A viscoplasticity theory applied to proportional and non-proportional cyclic loading at small strains. Int J Plast 20(8–9):1387–1401. doi:10.1016/j.ijplas.2003.07.002

Ellyin F, Golos K, Xia Z (1991) In-phase and out-of-phase multiaxial fatigue. J Eng Mater Technol-Trans ASME 113(1):112–118. doi:10.1115/1.2903365

Fatemi A, Shamsaei N (2011) Multiaxial fatigue: an overview and some approximation models for life estimation. Int J Fatigue 33(8):948–958. doi:10.1016/j.ijfatigue.2011.01.003

Feng ML, Ding F, Jiang YY (2006) A study of loading path influence on fatigue crack growth under combined loading. Int J Fatigue 28(1):19–27. doi:10.1016/j.ijfatigue.2005.04.002

Fremy F, Pommier S, Poncelet M, Raka B, Galenne E, Courtin S, Roux J-CL (2013) Load path effect on fatigue crack propagation in I + II + III mixed mode conditions—Part 1:

experimental investigations. Int J Fatigue (0). doi:http://dx.doi.org/10.1016/j.ijfatigue.2013.06.002

Hassan T, Taleb L, Krishna S (2008) Influence of non-proportional loading on ratcheting responses and simulations by two recent cyclic plasticity models. Int J Plast 24(10):1863–1889. doi:10.1016/j.ijplas.2008.04.008

Jiao F, Osterle W, Portella PD, Ziebs J (1995) Biaxial path-dependence of low-cycle fatigue behavior and microstructure of Alloy 800-H at room-temperature. Mater Sci Eng A-Struct 196(1–2):19–24. doi:10.1016/0921-5093(94)09690-2

Kanazawa K, Miller KJ, Brown MW (1977) Low-cycle fatigue under out-of-phase loading conditions. J Eng Mater Technol-Trans ASME 99(3):222–228

Karolczuk A (2006) Plastic strains and the macroscopic critical plane orientations under combined bending and torsion with constant and variable amplitudes. Eng Fract Mech 73(12):1629–1652. doi:10.1016/j.engfracmech.2006.02.005

Kida S, Itoh T, Sakane M, Ohnami M, Socie DF (1997) Dislocation structure and non-proportional hardening of Type 304 stainless steel. Fatigue Fract Eng Mater Struct 20(10):1375–1386. doi:10.1111/j.1460-2695.1997.tb01496.x

Kocanda S (1978) Fatigue failure of metals. Springer, Netherlands

Li J, Zhang ZP, Sun QA, Li CW (2011) Multiaxial fatigue life prediction for various metallic materials based on the critical plane approach. Int J Fatigue 33(2):90–101. doi:10.1016/j.ijfatigue.2010.07.003

Lipski A, Skibicki D (2012) Variations of the specimen temperature depending on the pattern of the multiaxial load—Preliminary research. Fatigue Fail Fract Mech 726:162–168. doi:10.4028/www.scientific.net/MSF.726.162

Little RE (1969) A note on shear stress criterion for fatigue failure under combined stress. Aeronaut Q 20:57

Liu KC, Wang JA (2001) An energy method for predicting fatigue life, crack orientation, and crack growth under multiaxial loading conditions. Int J Fatigue 23:129–134

Mcdiarmid DL (1986) Fatigue under out-of-phase bending and torsion. Fatigue Fract Eng Mater Struct 9(6):457–475

Mcdowell DL, Stahl DR, Stock SR, Antolovich SD (1988) Biaxial path dependence of deformation substructure of Type-304 Stainless-Steel. Metall Trans A 19(5):1277–1293. doi:10.1007/Bf02662589

Nakamura H, Takanashi M, Itoh T, Wu M, Shimizu Y (2011) Fatigue crack initiation and growth behavior of Ti-6Al-4V under non-proportional multiaxial loading. Int J Fatigue 33(7):842–848. doi:10.1016/j.ijfatigue.2010.12.013

Nishihara T, Kawamoto M (1945) The strength of metals under combined alternating bending and torsion with phase difference. Mem Coll Eng, Kyoto Imperial Univ 11:85–112

Nishino S, Hamada N, Sakane M, Ohnami M, Matsumura N, Tokizane M (1986) Microstructural study of cyclic strain-hardening behavior in biaxial stress states at elevated-temperature. Fatigue Fract Eng Mater Struct 9(1):65–77. doi:10.1111/j.1460-2695.1986.tb01212.x

Ohkawa I, Takahashi H, Moriwaki M, Misumi M (1997) A study on fatigue crack growth under out-of-phase combined loadings. Fatigue Fract Eng Mater Struct 20(6):929–940. doi:10.1111/j.1460-2695.1997.tb01536.x

Papadopoulos IV, Davoli P, Gorla C, Filippini M, Bernasconi A (1997) A comparative study of multiaxial high-cycle fatigue criteria for metals. Int J Fatigue 19(3):219–235. doi:10.1016/S0142-1123(96)00064-3

Qian J, Fatemi A (1996) Mixed mode fatigue crack growth: a literature survey. Eng Fract Mech 55(6):969–990. doi:10.1016/S0013-7944(96)00071-9

Rios ER, Andrews RM, Brown MW, Miller KJ (1989) Out-of-phase cyclic deformation and fatigue fracture studies on 316 stainless steel. In: Biaxial and multiaxial fatigue, EGF 3. Mechanical Engineering Publications

Rozumek D, Marciniak Z (2012) The investigation of crack growth in specimens with rectangular cross-sections under out-of-phase bending and torsional loading. Int J Fatigue 39:81–87. doi:10.1016/j.ijfatigue.2011.02.013

Shamsaei N, Fatemi A (2009) Effect of hardness on multiaxial fatigue behaviour and some simple approximations for steels. Fatigue Fract Eng Mater Struct 32(8):631–646. doi:10.1111/j.1460-2695.2009.01369.x

Shamsaei N, Fatemi A, Socie DF (2010a) Multiaxial cyclic deformation and non-proportional hardening employing discriminating load paths. Int J Plast 26(12):1680–1701. doi:10.1016/j.ijplas.2010.02.006

Shamsaei N, Gladskyi M, Panasovskyi K, Shukaev S, Fatemi A (2010b) Multiaxial fatigue of titanium including step loading and load path alteration and sequence effects. Int J Fatigue 32(11):1862–1874. doi:10.1016/j.ijfatigue.2010.05.006

Simburger A (1975) Festigkeitsverhalten zaher Werkstoffe bei einer mehrachsigen, phasenverschobenen Schwingbeanspruchung mit korperfesten und veranderlichen Hauptspannungsrichtungen. Bericht nr. FB-121. Laboratorium fur Betriebsfestigkeit, Darmstadt

Skibicki D, Dymski S (2010) The influence of fatigue loading on the microstructure of an austenitic stainless steel. Mater Test-Mater Compon Technol Appl 52(11–12):787–794

Skibicki D, Sempruch J, Pejkowski L (2012) Steel X2CrNiMo17-12-2 testing for uniaxial, proportional and non-proportional loads as delivered and in the annealed condition. Fatigue Fail Fract Mech 726:171–180. doi:10.4028/www.scientific.net/MSF.726.171

Socie DF (1996) Fatigue damage simulation models for multiaxial loading. In: Proceedings of the sixth international fatigue congress. Pergamon, New York, pp 967–976

Socie DF, Marquis GB (2000) Multiaxial fatigue. Society of Automotive Engineers

Sonsino CM (1983) Schwingfestigkeitsverhalten von Sinterstahl unter kombinierten mehrachsiger phasegleichen und phasenverschobenen Beanspruchungszustande. Bericht Nr FB-168. LBF Darmstat

Verreman Y, Guo H (2007) High-cycle fatigue mechanisms in 1045 steel under non-proportional axial-torsional loading. Fatigue Fract Eng Mater Struct 30(10):932–946. doi:10.1111/j.1460-2695.2007.01164.x

Xiao L, Kuang ZB (1996) Biaxial path dependence of macroscopic response and microscopic dislocation substructure in type 302 stainless steel. Acta Mater 44(8):3059–3067. doi:10.1016/1359-6454(95)00441-6

Xiao L, Umakoshi Y, Sun J (2000) Biaxial low cycle fatigue properties and dislocation substructures of zircaloy-4 under in-phase and out-of-phase loading. Mater Sci Eng A-Struct 292(1):40–48. doi:10.1016/S0921-5093(00)01005-4

Zenner H, Simburger A, Liu JP (2000) On the fatigue limit of ductile metals under complex multiaxial loading. Int J Fatigue 22(2):137–145. doi:10.1016/S0142-1123(99)00107-3

Zhang JX, Jiang YY (2005) An experimental investigation on cyclic plastic deformation and substructures of polycrystalline copper. Int J Plast 21(11):2191–2211. doi:10.1016/j.ijplas.2005.02.004

http://www.springer.com/978-3-319-01564-4

Phenomena and Computational Models of
Non-Proportional Fatigue of Materials
Skibicki, D.
2014, VIII, 126 p. 84 illus., 5 illus. in color., Softcover
ISBN: 978-3-319-01564-4